Master Sciences de la matière
École Normale Supérieure de Lyon
Université Claude Bernard Lyon I

Internship 2023-2024
Albouy Alice
M2 Physics

NANOGrav constraints on an axion spectator field during cosmic inflation

Abstract : The need for a richer structure in the inflation sector motivates the study of an inflationary model where inflation is driven by a single inflaton field to which is added a spectator axion-like field coupled to an abelian gauge field. This work is the study of such an inflationary axion-$U(1)$ spectator model in the low-backreaction regime where the energy density stored in the gauge field is negligible compared to the energy density stored in the axion-like field. The dynamics of the axion-like field is studied and this study allows to introduce an important parameter denoted δ that is approximately a measure of the relative change of the axion-like field value during one Hubble time at the top of its potential and that is taken equal to $\delta = 0.2, 0.5$. The study of the dynamics of the gauge field reveals that a tachyonic mass term, that depends on the coupling between the axion-like field and the gauge field, appears in the equation of motion of the plus polarization of the gauge field at large scales. Wentzel Kramers Brouillouin approximation is used to derive an approximate solution that results in an exponentially amplified plus polarization of the gauge field. Perturbation theory is used to study tensor perturbations of the metric. It appears that the gradients of the gauge field source tensor perturbations, that lead to gravitational waves (GWs). The GW spectrum is thus computed and the results from this work indicate that the GW spectrum is highly chiral. Inflationary GWs can also be detected by measuring the correlated pulse time arrival delays between pulsars. The NANOGrav collaboration used this technique called pulsar timing array (PTA) to recently release a PTA data set yielding a strong evidence of a GW spectrum that is consistent with a spectrum from a population of supermassive black-hole binaries (SMBHBs). However, more exotic cosmological sources, as the coupling between an axion-like field and an abelian gauge field during inflation, can not excluded. This work uses the software PTArcade to perform a Bayesian statistical analysis of the inflationary axion-$U(1)$ spectator model with the PTA data collected by the NANOGrav collaboration. The results from the 68% Bayesian credible regions are the following. In order for the GW spectrum produced by the inflationary axion-$U(1)$ spectator model to fit PTA data and improve the SMBHB model, the parameter δ should be taken equal to 0.2, $\Delta N = 17$ e-folds should separate the moment when the CMB scale leaves the horizon and the moment when the axion velocity is maximal, the fine structure constant α of the $U(1)$ sector should satisfy $46 < \alpha < 66$, the Hubble rate H should verify $7.73 \cdot 10^{11}\text{GeV} < H < 4.23 \cdot 10^{13}\text{GeV}$ but this constraint depends only on the choice of the prior distributions of the free parameters, the parameters α and H should be related via $\alpha = -4\log_{10}(1.68 \cdot 10^{-29} H^2) + 46$ and the height of the axion potential Λ^4 should verify $9.20 \cdot 10^{14}\text{GeV} < \Lambda < 1.16 \cdot 10^{16}\text{GeV}$. For $\delta = 0.5$, the inflationary axion-$U(1)$ spectator model can explain PTA data if $\Delta N = 15$, $19.6 < \alpha < 28.4$, $7.73 \cdot 10^{11}\text{GeV} < H < 4.23 \cdot 10^{13}\text{GeV}$, $\alpha = -1.76\log_{10}(1.68 \cdot 10^{-29} H^2) + 19.6$ and $1.16 \cdot 10^{15}\text{GeV} < \Lambda < 2.06 \cdot 10^{16}\text{GeV}$ but this choice of parameters does not improve the SMBHB model. For $\delta = 0.2$, in order for the inflationary axion-$U(1)$ spectator model together with the SMBHB model to fit PTA data and improve the SMBHB model, the parameters ΔN, α, H and Λ^4 must be subjects to the same constraints as in the case of the inflationary axion-$U(1)$ spectator model alone and the parameters A and γ of the SMBHB contribution are not constrained. For $\delta = 0.5$, in order for the inflationary axion-$U(1)$ model together with the SMBHB model to fit PTA data and improve the SMBHB model, the parameters ΔN, α, H and Λ^4 are not constrained but the region $\gamma > 5, \log_{10}(A) < -15$ should be excluded. Finally, this work allows to conclude that amongst all the models tested, the inflationary axion-$U(1)$ spectator model together with the SMBHB model with $\delta = 0.2$ is the one that improves the most the SMBHB model.

Key words : *cosmic inflation, inflaton field, axion-like field, abelian gauge field, tachyonic instability, tensor perturbations, gravitational waves, pulsar timing array, Bayesian statistical analysis*

Internship tutor :
Kai Schmitz
kai.schmitz@uni-muenster.de
Institute for Theoretical Physics
Wilhelm-Klemm-Strasse 9
48149 Münster
GERMANY

Acknowledgments

I want to thank the whole Particle Cosmology Münster group for making me feel so welcome and for the interesting discussions about my work as well as academia I had with all of them. They treated me as a full member of the group, creating a very lively environment that allowed me to carry out my Master project in the best possible conditions. I thank Levin Wessing with whom I shared the office during my stay. I thank him for his understanding and flexibility and for making me feel comfortable in our office. I thank Tobias Schröder who showed interest in my work and asked me interesting questions. I particularly thank him for the time he took to explain me as best as he could PTA data analysis. I thank David Esmyol who helped me getting the NANOGrav free spectrum and therefore without whom I would not have been able to get a major result for my project. I thank Oleksandr Sobol who was always ready to help me and took a particularly long time to help me deriving the solution of the equation of motion of the gauge field using WKB approximation. I feel particularly thankful to Richard von Eckardstein. At the beginning of my stay, he was not really supposed to take part in my project but by asking him so many questions and because he took a lot of time to answer to these questions, he contributed a lot to my project. I want to thank him for this time he took for me and for learning me many things about cosmology. I thank Katrin Greve, Edoardo Spezzano and Jan Knetsch who had always supporting words to me and became my friends. Finally, I deeply thank Kai Schmitz, my supervisor, without whom this project could not have been possible. He learnt me many things about inflation and NANOGrav data analysis, he was always available to answer to my questions and gave me some freedom in my project. I thank him for his trust and for the very interesting project he suggested me.

Notations and conventions

The present work uses natural units: the speed of light in vacuum c and the Planck constant $\hbar$ are reduced to unity. The only base quantity becomes the energy such that [mass] = [energy]. M_P denotes the reduced Planck mass given by $M_P = 1/\sqrt{8\pi G_N} = 2.4 \cdot 10^{18}$GeV with G_N the gravitational constant.
Greek indices running from 0 to 3 are used for four-vectors (e.g. x^μ). Latin indices denote spatial indices and three-vectors are denoted with an arrow. Einstein summation convention in which summation over repeated indices of which one is an upper index and one is a lower index is assumed.
For a 3-vector $\vec{a}$, a denotes the norm of $\vec{a}$.
Partial derivatives are denoted as :

$$\partial_\mu \equiv \frac{\partial}{\partial x^\mu} = \left(\frac{\partial}{\partial x^0}, \vec{\nabla} \equiv \left(\frac{\partial}{\partial x^1}, \frac{\partial}{\partial x^2}, \frac{\partial}{\partial x^3} \right) \right). \tag{0.1}$$

This work uses the standard cosmological model ΛCDM where CDM stands for Cold Dark Matter. The ΛCDM model is based on the assumption that the distribution of matter in the universe is spatially homogeneous and isotropic. Since this work is in the general relativity framework, the universe is modelled by a four-dimensional manifold equipped with a tensor field g called metric. The definition of g yields to the definition of the interval $ds^2 = g_{\mu\nu} dx^\mu dx^\nu$ which describes the physically measured lengths and times. This work uses the Friedmann-Lemaître-Robertson-Walker (FLRW) spacetime described by the interval :

$$ds^2 = -dt^2 + a^2(t) d\vec{x}^2, \tag{0.2}$$

with $a(t)$ the scale factor. This definition leads to the FLRW metric $g_{\mu\nu}$=Diag(-1,$a^2(t)$,$a^2(t)$,$a^2(t)$). Note that the curvature is always set to zero.
The conformal time is denoted τ and is defined as:

$$d\tau \equiv \frac{dt}{a(t)}. \tag{0.3}$$

With this definition, the interval ds^2 becomes:

$$ds^2 = -a^2(\tau)(d\tau^2 - d\vec{x}^2). \tag{0.4}$$

Derivatives with respect to time t are denoted with a dot and derivatives with respect to conformal time τ are denoted with a prime.
This work takes place during cosmic inflation and assumes a de Sitter stage. This means that in the description of a perfect fluid, the equation of state takes the form $P = -\rho$ with P the pressure and ρ the energy density. As a consequence, the dominant contribution to the total energy density is constant in time as well as the Hubble parameter $H(t) \equiv \dot{a}(t)/a(t)$ that is simply denoted by H. The scale factor is given by:

$$a(t) = a_I \exp H(t - t_I) \Rightarrow a(\tau) = -\frac{1}{H\tau}, \tag{0.5}$$

with a_I some constant and t_I the time at which inflation starts.
If not specified, four-vectors represent physical fields with indices raised and lowered with the metric $g_{\mu\nu}$. For instance, for a field A_μ (dropping the dependence in τ and $\vec{x}$):

$$A_\mu = (-A^0, \vec{A}) \quad A^\mu = \left(\frac{A^0}{a^2}, \frac{\vec{A}}{a^2} \right). \tag{0.6}$$

The "electric" and "magnetic" fields are related to the $U(1)$ gauge field A_μ by:

$$a^2(\tau)\vec{B}(\tau, \vec{x}) = \vec{\nabla} \times \vec{A}(\tau, \vec{x}) \quad a^2(\tau)\vec{E}(\tau, \vec{x}) = -\partial_\tau \vec{A}(\tau, \vec{x}). \tag{0.7}$$

If not specified, the Coulomb gauge in which $\vec{\nabla} \cdot \vec{A} = 0$ is assumed as well as the temporal gauge in which $A_0 \equiv 0$.
The electromagnetic tensor or field strength tensor is denoted $F_{\mu\nu}$ and is given by $F_{\mu\nu} = \partial_\mu A_\nu - \partial_\nu A_\mu$. This gives:

$$F_{\mu\nu} = a^2(\tau) \begin{bmatrix} 0 & E_1 & E_2 & E_3 \\ -E_1 & 0 & B_3 & -B_2 \\ -E_2 & -B_3 & 0 & B_1 \\ -E_3 & B_2 & -B_1 & 0 \end{bmatrix}. \tag{0.8}$$

The electromagnetic Hodge dual tensor is defined as $\tilde{F}^{\mu\nu} = (1/2)\epsilon^{\mu\nu\rho\sigma} F_{\rho\sigma}$ with $\epsilon^{0123} = +1$.
The comoving wavenumber k is related to the comoving wavelenght λ via:

$$k = \frac{2\pi}{\lambda}, \tag{0.9}$$

and is positive. Therefore, all integrals over comoving wavenumber that appear without bounds are considered being over all real positive numbers. What is called scale is the comoving wavelenght λ and therefore a large scale corresponds to a small comoving wavenumber k.

Contents

1 Introduction

The North American Nanohertz Observatory for Gravitational Waves (NANOGrav) has recently released its 15-year pulsar timing array (PTA) data set that yields a strong evidence for a stochastic gravitational wave (GW) background signal that is correlated among 67 pulsars [1]. The inferred GW background amplitude and spectrum are consistent with astrophysical expectations for a signal from a population of supermassive black-hole binaries (SMBHBs) [2]. However more exotic cosmological sources can not be excluded, as e.g., scalar induced GWs, a cosmological phase transition, or cosmic defects in the form of cosmic strings or domain walls [3]. Another well-known source of GWs from the early universe are primordial GWs from cosmic inflation. How about this possibility? Can GWs from cosmic inflation be responsible for the NANOGrav signal? This question is at the heart of this work.

The standard Λ cold dark matter (ΛCDM) model is based on the paradigm of inflationary cosmology where inflation denotes a stage of quasi-exponential expansion of the universe before the hot Big Bang. Inflation has been introduced in order to solve problems of old-school Big Bang cosmology such as the horizon and flatness problems. On top, inflation brings other interesting features: it sources scalar and tensor perturbations as vacuum fluctuations [4–7]. The inflationary exponential expansion of the universe excites quantum fields and stretches their perturbations to cosmological scales, that become classical on these large scales, inducing energy fluctuations. Once stretched to cosmological scales, these perturbations leave the horizon and freeze out. They re-enter the observable universe during the reheating stage after inflation, in the same state as when they left the horizon during inflation, thus carrying information about inflation. It is believed that primordial scalar perturbations lead to cosmic microwave background (CMB) anisotropies and the large-scale structure of the universe while primordial tensor perturbations from inflation lead to inflationary GWs. These are quantities that can be measured and thus that can give information about the early universe.

Nowadays, there is no consensus on the microscopic origin of inflation in field or string theory. There exists many inflationary models, the most popular being chaotic inflation, R^2 inflation or alpha attractors. However, many of these models are toy models that consist of one scalar field, the inflaton, in a specific potential. Comparing such models with for instance the standard model of particle physics, a richer structure in the inflation sector, namely more degrees of freedom, could be expected. In addition, the degrees of freedom involved during inflation have to decay into standard model of particle physics degrees of freedom during the reheating stage, giving another motivation to add degrees of freedom to inflationary models. A promising type of degree of freedom is the axion field. The axion field is a pseudo-Nambu-Goldstone boson associated with the spontaneous breaking of a global and anomalous $U(1)$ symmetry. The axion field has originally been invented in the context of quantum chromodynamics (QCD) in order to solve the strong CP problem [8–11]. However, this work is not concerned with the QCD axion field but with an axion-like field in a more general sense. For simplicity, this axion-like field will be referred to as the axion field. The axion field comes with a shift symmetry and therefore can couple with $U(1)$ gauge fields via the coupling $\alpha(\sigma/4f)F_{\mu\nu}\tilde{F}^{\mu\nu}$ where $F_{\mu\nu}$ is the electromagnetic field strength tensor and $\tilde{F}^{\mu\nu} = (1/2)\epsilon^{\mu\nu\rho\sigma}F_{\rho\sigma}$ with $\epsilon^{0123} = +1$ is the electromagnetic Hodge dual tensor. Such a coupling adds a tachyonic mass term in the equation of motion of the gauge field, leading to an interesting phenomenology such as explosive gauge field production which in turn can source tensor perturbations and thus GWs [12–16]. This gives the idea of studying an inflationary model where inflation is driven by an inflaton field and add an axion field that is spectator and coupled to a $U(1)$ gauge field. The tensor perturbations produced by such a coupling experience the same phenomenon as the vacuum perturbations produced during inflation: the inflationary exponential expansion of the universe stretches these tensor perturbations to cosmological scales that become classical, leave the horizon and freeze out. They re-enter the observable universe during the reheating stage after inflation carrying information about their source that is in this case the axion-$U(1)$ gauge field coupling. From an inflationary model with a spectator axion field coupled to a $U(1)$ gauge field, an extra GW contribution on top of the vacuum contribution is therefore expected.

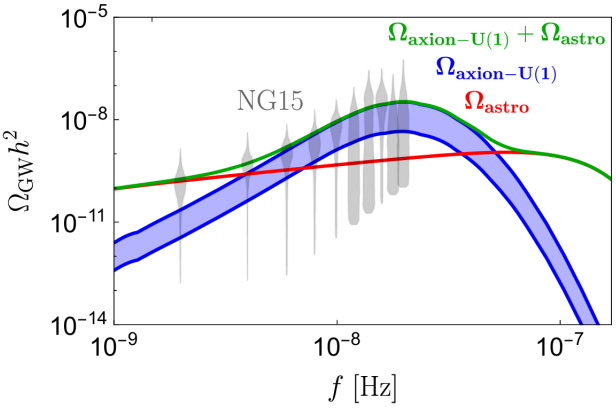

Figure 1: Qualitative comparison of the GW spectrum sourced by an inflationary model with spectator axion coupled to a $U(1)$ gauge field with recent NANOGrav data presented in [17]. The supermassive black hole binaries contribution is also displayed.

This work presents such an inflationary axion-$U(1)$ spectator model where inflation is driven by an inflaton field and where a rolling spectator axion is coupled to a $U(1)$ gauge field. The aim of this work is to derive the GW spectrum produced by this inflationary axion-$U(1)$ spectator model and give constraints on the free parameters of the model in order for the resulting GW spectrum to explain the recent PTA data. The PTA data set studied in this work is the PTA data set collected by the NANOGrav collaboration. The motivation of this project is the work of Caner Unal, Alexandros Papageorgiou and Ippei Obata [17] where the GW spectrum from such an inflationary axion-$U(1)$ spectator model is qualitatively compared to PTA data. It is claimed in [17] that from Fig.1, that consists in plotting the GW spectrum sourced by such an inflationary axion-$U(1)$ spectator model on top of recent PTA data, this GW spectrum can explain PTA data. However, this result

lying on no data analysis, the idea of this project is to use recent PTA data to add constraints on the free parameters of the inflationary axion-$U(1)$ spectator model via a proper statistical analysis such that for values of the free parameters that satisfy these constraints, the resulting GW spectrum could explain PTA data.
The outline of this work is the following. The first chapter introduces the inflationary axion-$U(1)$ spectator model: the action is defined as well as the axion potential and the equations of motion for the axion field and the gauge field are derived and solved. The second chapter is the study of the production of tensor perturbations. The tensor perturbations of the metric are introduced and their evolution is studied. The tensor power spectrum, being the observable, is computed. The second chapter also presents a discussion on the domain of validity of this work. The last chapter is dedicated to PTA data analysis using the software PTArcade. PTArcade allows to perform a Bayesian statistical analysis of the inflationary axion-$U(1)$ spectator model with the PTA data set collected by the NANOGrav collaboration. The results from the data analysis are presented and discussed. Constraints on the free parameters of the inflationary axion-$U(1)$ spectator model for which the sourced GW spectrum could explain PTA data are derived. The fit to PTA data from the GWs produced by the inflationary axion-$U(1)$ spectator model is compared to the fit to PTA data from GWs produced by the SMBHB model. Finally, the scenario of GWs sourced by two contributions simultaneously, the inflationary axion-$U(1)$ spectator model and the SMBHB model is studied.

2 Characterization of the system

This section presents the model studied in this work, which is an inflationary axion-$U(1)$ spectator model from [18]. The dynamics of the spectator sector, namely the axion and the gauge field, are studied following [18].

2.1 The inflationary axion-$U(1)$ spectator model

This work is the study of an inflationary model where inflation is driven by an inflaton ϕ. A rolling axion σ is considered as spectator and is coupled to a $U(1)$ gauge field A_μ[1] with field strength tensor $F_{\mu\nu}$. With the FLRW metric $g_{\mu\nu}$, the action describing the system then takes the form:

$$S = \int d^4x \left[\sqrt{-\det(g_{\mu\nu})}\left(\frac{M_P^2}{2}R - \frac{1}{2}g^{\mu\nu}\partial_\mu\phi\partial_\nu\phi - \frac{1}{2}g^{\mu\nu}\partial_\mu\sigma\partial_\nu\sigma - V(\phi,\sigma) - \frac{1}{4}F_{\mu\nu}F^{\mu\nu}\right) - \alpha\frac{\sigma}{4f}F_{\mu\nu}\tilde{F}^{\mu\nu}\right], \tag{2.1}$$

with $\det(g_{\mu\nu})$ the determinant of the metric $g_{\mu\nu}$, R the Ricci scalar, α the fine structure constant of the $U(1)$ sector that the axion σ couples to, and f the decay constant of the axion σ. This model will be referred to as the inflationary axion-$U(1)$ spectator model.
Assuming no direct coupling between the inflaton ϕ and the axion σ, one can decompose the potential $V(\phi,\sigma)$ into two independent contributions:

$$V(\phi,\sigma) = V_\phi(\phi) + V_\sigma(\sigma). \tag{2.2}$$

In this work, the inflaton potential $V_\phi(\phi)$ is let unspecified. The axion potential $V_\sigma(\sigma)$ is given in Fig.2. It corresponds to the simple and typical potential for an axion [2], where the parameter Λ characterizes the height of the potential:

$$V_\sigma(\sigma) = \frac{\Lambda^4}{2}\left[\cos\left(\frac{\sigma}{f}\right) + 1\right], \tag{2.3}$$

and has a maximum in $\sigma = 0$ and a minimum in $\sigma = f\pi$. This axion potential allows for a small axion velocity $\dot{\sigma}$ at early and late times with a maximal velocity at $\sigma = (\pi/2)f \equiv \sigma_*$. So if the axion σ is slightly displaced from its maximum, it can slowly roll down its potential. For now on, the time at which $\sigma = \sigma_*$ will be denoted t_* and any quantity labelled with a star denotes the quantity evaluated at $t = t_*$.

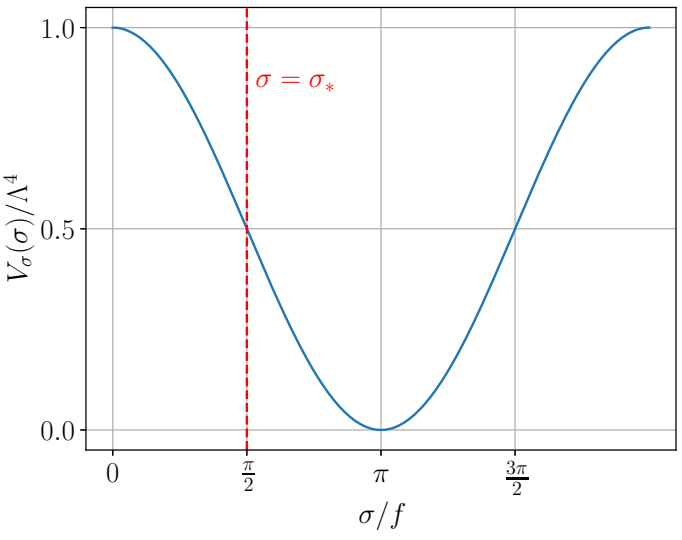

Figure 2: The axion potential $V_\sigma(\sigma)$

In order for the inflaton field to drive inflation, the spectator sector (the axion σ and the gauge field $\vec{A}$) must provide a subleading contribution to the total energy density during inflation. It is therefore assumed that $\rho_A, \rho_\sigma \ll \rho_\phi$ where $\rho_X \equiv \dot{X}^2/2 + V_X(X)$ denotes the energy density of the field $X = \sigma, \phi$ and ρ_A denotes the energy density of the gauge field $\vec{A}$. This consideration leads to the approximate Friedmann equation: $3M_P^2H^2 = \rho_\phi$. In addition, a quasi de Sitter stage is assumed, meaning $\dot{\phi}^2/2 + V_\phi(\phi) = \rho_\phi = -P(\phi) = -\dot{\phi}^2/2 + V_\phi(\phi) \Rightarrow \dot{\phi} \ll 1$. This is known as the slow-roll condition of the

[1] In the following, the gauge field A_μ will be denoted $\vec{A}$ as this work takes place in the temporal gauge.
[2] Potentials of this type are created by instantons in strongly coupled gauge theories that the axion may couple to.

inflaton field. Moreover, to ensure a sufficiently long de Sitter stage, and so a sufficiently long inflaton slow-roll, the potential $V_\phi(\phi)$ is assumed being very flat so that the Hubble rate H can be considered as constant.
This work takes place in the low-backreaction regime in which it is assumed that the backreaction of the gauge field $\vec{A}$ onto the axion σ is negligible which translates into the assumption $\rho_A \ll \rho_\sigma$.

2.2 Dynamics of the axion field

This section is dedicated to the study of the dynamics of the axion σ in the low-backreaction regime.
The low-backreaction regime translates into the fact that the contribution of the coupling term $\sigma F_{\mu\nu}\tilde{F}^{\mu\nu}$ (see Eq. (2.1)) between the axion σ and the gauge field $\vec{A}$ is assumed to be sufficiently small to be neglected in the dynamics of the axion σ. In addition, the axion slow-roll imposes that $\ddot{\sigma} \ll 1$ in order to ensure that the axion velocity $\dot{\sigma}$ evolves slowly. Finally, it is assumed that at the beginning of inflation, at times t of order $t \sim 1/M_P$, the space-time is homogeneous so that $\sigma = \sigma(t)$. Is is assumed that the expansion of the universe during inflation is sufficiently strong that the axion σ can be considered homogeneous at all times during inflation.
Taking these restrictions into account, one can derive the equation of motion of the axion σ by varying the action given in Eq. (2.1) with respect to σ and setting it to zero. This leads to:

$$3H\dot{\sigma}(t) + \frac{\Lambda^4}{2f}\sin\frac{\sigma(t)}{f} = 0. \tag{2.4}$$

An integration gives the slow-roll solution for the axion σ:

$$\sigma(t) = 2f\arctan\left[e^{\delta H(t-t_*)}\right], \quad \delta \equiv \Lambda^4/(6H^2f^2). \tag{2.5}$$

Expanding the axion potential and defining the field distance traversed by the axion σ during one Hubble time as $\Delta\sigma \sim \dot{\sigma}/H$ leads to $3H^2\Delta\sigma \sim (\Lambda^4/2f^2)\sigma$. This means that $\delta \sim \Delta\sigma/\sigma$ i.e. the parameter δ is approximately a measure of the relative change of the axion value during one Hubble time at the top of the potential.
Using the solution Eq. (2.5), the slow roll condition of the axion σ becomes:

$$\left|\frac{\ddot{\sigma}}{3H\dot{\sigma}}\right| \ll 1 \Rightarrow \delta << 3. \tag{2.6}$$

This condition motivates to choose two values of reference for the parameter δ in the following: $\delta = 0.2$ and $\delta = 0.5$. In addition, earlier studies also considered these two values, which facilitates the comparison between the results obtained in this work and existing numerical results in literature.
Finally, an important parameter of the model is the dimensionless parameter ξ defined as:

$$\xi(t) \equiv \frac{\alpha\dot{\sigma}(t)}{2fH} = \frac{2\xi_*}{\left(a(t)/a_*\right)^\delta + \left(a_*/a(t)\right)^\delta}, \tag{2.7}$$

where $\xi_* = \alpha\delta/2$ is the maximum of ξ. Without loss of generality, ξ_* is assumed being strictly positive.

2.3 Amplification of the gauge field

In this section, the dynamics of the gauge field $\vec{A}$ is studied. The calculation follows closely [18]. It is shown that because the gauge field $\vec{A}$ is coupled to the axion σ with non-vanishing velocity, one polarization of the gauge field $\vec{A}$ is exponentially amplified.

2.3.1 Equation of motion of the gauge field

In order to study the dynamics of the gauge field $\vec{A}$, the first step is to derive its equation of motion. This is what is presented in this section.

NB: *For now on, all equations are derived in term of the conformal time τ, see the Notation and Convention section for more details.*

Varying the action given in Eq. (2.1) with respect to the gauge field $\vec{A}$ and equating it to zero yields the equation of motion of the gauge field $\vec{A}$, making use of the definition of the electromagnetic tensor (see the Notation and Convention section for more details):

$$\left(\frac{\partial^2}{\partial\tau^2} - \vec{\nabla}^2 - \frac{\alpha\sigma'(\tau)}{f}\vec{\nabla}\times\right)\vec{A}(\tau,\vec{x}) = 0. \tag{2.8}$$

Promoting the gauge field $\vec{A}$ into an operator $\hat{\vec{A}}$ and quantizing it leads to the definition:

$$\hat{A}_i(\tau,\vec{x}) \equiv \sum_{\lambda=\pm}\int \frac{d^3k}{(2\pi)^{3/2}} e^{i\vec{k}\cdot\vec{x}}\hat{A}_\lambda(\tau,\vec{k}) = \sum_{\lambda=\pm}\int \frac{d^3k}{(2\pi)^{3/2}} e^{i\vec{k}\cdot\vec{x}}\left[\epsilon_i^\lambda(\hat{k})A_\lambda(\tau,k)\hat{a}_\lambda(\vec{k}) + \epsilon_i^{\lambda *}(-\hat{k})A_\lambda(\tau,k)\hat{a}_\lambda^\dagger(-\vec{k})\right], \tag{2.9}$$

where $\lambda = \pm$ denotes the polarization, $\hat{A}_\lambda(\tau,\vec{k})$ is the mode operator associated to the gauge field operator $\hat{\vec{A}}$, $A_\lambda(\tau,k)$ is the mode function associated to the gauge field operator $\hat{\vec{A}}$, $\vec{\epsilon}^\lambda(\vec{k})$ is the polarization vector satisfying:

$$\vec{\epsilon}_\lambda^*(\vec{k}) = \vec{\epsilon}_{-\lambda}(\vec{k}) = \vec{\epsilon}_\lambda(-\vec{k}) \quad \vec{k}\cdot\vec{\epsilon}^\lambda(\vec{k}) = 0 \quad \vec{\epsilon}_\lambda^*(\vec{k})\cdot\vec{\epsilon}_{\lambda'}(\vec{k}) = \delta_{\lambda\lambda'} \quad i\vec{k}\times\vec{\epsilon}^\lambda(\vec{k}) = \lambda k\vec{\epsilon}^\lambda(\vec{k}), \tag{2.10}$$

and $\hat{a}_\lambda^\dagger(\vec{k})$, $\hat{a}_\lambda(\vec{k})$ are respectively the creation and annihilation operators for the gauge field operator $\hat{\vec{A}}$ satisfying the commutation relation $[\hat{a}_\lambda(\vec{k}),\hat{a}_{\lambda'}^\dagger(\vec{p})] = \delta_{\lambda\lambda'}\delta^{(3)}(\vec{k}-\vec{p})$. From Eq. (2.8), one can derive the equation of motion of the mode function A_λ that takes the form:

$$A_\pm''(\tau,k) + \left(k^2 \pm k\frac{2\xi(\tau)}{\tau}\right)A_\pm(\tau,k) = 0 \Rightarrow A_\pm''(\tau,k) + \left(k^2 \pm \frac{4k\xi_*}{\tau\left[(\tau/\tau_*)^\delta + (\tau_*/\tau)^\delta\right]}\right)A_\pm(\tau,k) = 0. \tag{2.11}$$

The equation of motion of the mode function A_λ given in Eq. (2.11) is the standard dispersion relation with the extra term $\lambda k(2\xi(\tau)/\tau)A_\lambda(\tau,k)$ that depends on the axion-$U(1)$ coupling controlled by the parameter ξ that depends in turn on the axion velocity σ'. For $\lambda = +$, this term becomes a tachyonic mass term and therefore one can already anticipate that the mode function of plus polarization A_+ solution of Eq. (2.11) will be exponentially growing. More precisely, for $\lambda = +$, the term $\lambda k(2\xi(\tau)/\tau)A_\lambda(\tau,k)$ becomes a tachyonic mass term for comoving wavenumbers k that satisfy $k \leq 2\xi(\tau)a(\tau)H$. Moreover, the structure of Eq. (2.8) introduces a critical comoving wavenumber denoted $k_* = -\tau_*^{-1}$. This critical comoving wavenumber corresponds to the scale that leaves the horizon at $\tau = \tau_*$ i.e. when the axion velocity is maximal and thus corresponds to the time at which the tachyonic mass term is maximal. Therefore, tachyonic instability occurs at large scales. This means that for scales deep inside the horizon i.e. scales much smaller than the size of the horizon, the tachyonic mass term can be neglected and the dispersion relation follows the standard dispersion relation. However, for comoving wavenumbers $k \leq 2\xi(\tau)a(\tau)H$, i.e. at large scales, the mode A_+ indeed gets a tachyonic mass term, that is therefore exponentially amplified. This amplification can be interpreted as the production of quanta of the gauge field of plus polarization [19, 20]. As the mode A_+ is the only amplified mode, for now on the mode A_- can be neglected.
To sum up, because the gauge field $\vec{A}$ is coupled to the axion σ with non-vanishing velocity, one polarization of the gauge field $\vec{A}$ is exponentially amplified leading to the production of quanta of the gauge field. The next section consists in solving explicitly the equation of motion of the gauge field mode function A_+ and show that it is indeed exponentially amplified.

2.3.2 Solution of the equation of motion of the gauge field: Wentzel Kramers Brouillouin approximation

The equation of motion of the mode function A_+ given in Eq. (2.11) can not be analytically solved. The common way in literature of solving such an equation is to use the semi-analytical method called Wentzel Kramers Brouillouin (WKB) approximation. This is what is done in this section.

NB: *For convenience, in this section the derivative with respect to the variable x will be denoted by a prime even though x does not denote the conformal time.*

Semi-analytical method For a differential equation of the form:

$$\lambda^2\frac{d^2A(x)}{dx^2} + Q(x)A(x) = 0, \tag{2.12}$$

with parameter λ and

$$Q(x) = \begin{cases} p(x)^2 & , x > \bar{x} \\ -q(x)^2 & , x < \bar{x}, \end{cases} \tag{2.13}$$

where the point $\bar{x}$ is called the classical turning point, one can make the Ansatz that the solution takes the form:

$$A(x) = \exp\left[\frac{1}{\lambda}\sum_{n=0}^{\infty}\lambda^n S_n(x)\right], \tag{2.14}$$

with $S_n(x)$ some functions to be determined.
The WKB approximation consists in considering only the terms in first order in λ such that Eq. (2.12) can be approximated as, replacing the function A by the expression given in Eq. (2.14):

$$S_0'^2(x) + 2\lambda S_0'(x)S_1'(x) + \lambda S_0''(x) + Q(x)\mathcal{O}(\lambda^2) = 0. \tag{2.15}$$

Equating each term in power of λ to zero yields two equations:

$$\begin{cases} S_0'^2(x) + Q(x) = 0 \\ 2S_0'(x)S_1'(x) + S_0''(x) = 0. \end{cases} \tag{2.16}$$

From here, two distinct cases arise: $x > \bar{x}$ and $x < \bar{x}$.

$x > \bar{x}$

For $x > \bar{x}$, according to Eq. (2.13), the function $Q(x)$ is strictly positive leading to:

$$S_0(x) = \pm i \int_{\bar{x}}^{x} p(x')dx' + C_0^{\pm}, \tag{2.17}$$

where $C_0^{\pm}$ are integration constants. Inserting this last equation into the second equation of Eq. (2.16) yields:

$$S_1(x) = -\frac{1}{2}\ln p(x) + C_1, \tag{2.18}$$

with C_1 an integration constant. Eq. (2.17) and Eq. (2.18) allow to write the function A as, where α_1 and β_1 are complex constants that encapsulate the integration constants and the phase $\pi/4$ is added for convenience (note that the minus sign appears by convention):

$$A(x) = \frac{\alpha_1}{\sqrt{p(x)}}\cos\left(\frac{1}{\lambda}\int_{\bar{x}}^{x} p(x')dx' + \frac{\pi}{4}\right) - \frac{\beta_1}{\sqrt{p(x)}}\sin\left(\frac{1}{\lambda}\int_{\bar{x}}^{x} p(x')dx' + \frac{\pi}{4}\right). \tag{2.19}$$

The solution given in Eq. (2.19), setting λ to 1, is known as the WKB solution in the regime $x > \bar{x}$.

$x < \bar{x}$

For $x < \bar{x}$, according to Eq. (2.13), the function $Q(x)$ is strictly negative leading to:

$$S_0(x) = \pm \int_{x}^{\bar{x}} q(x)dx + D_0^{\pm}, \tag{2.20}$$

where $D_0^{\pm}$ are integration constants. Inserting this last equation into the second equation of Eq. (2.16) yields:

$$S_1(x) = -\frac{1}{2}\ln q(x) + D_1, \tag{2.21}$$

with D_1 an integration constant. Eq. (2.20) and Eq. (2.21) allow to write the function A as, where α_2 and β_2 are complex constants that encapsulate the integration constants (note that the minus sign appears by convention):

$$A(x) = \frac{\alpha_2}{\sqrt{q(x)}}\exp\left(-\frac{1}{\lambda}\int_{x}^{\bar{x}} q(x')dx'\right) - \frac{\beta_2}{\sqrt{q(x)}}\exp\left(\frac{1}{\lambda}\int_{x}^{\bar{x}} q(x')dx'\right). \tag{2.22}$$

The solution given in Eq. (2.22), setting λ to 1, is known as the WKB solution in the regime $x < \bar{x}$.

It is important to stress here that WKB approximation is valid in the regimes $|p'(x)| \ll p^2(x)$ and $|q'(x)| \ll q^2(x)$ [21]. WKB approximation thus breaks down if p, q vanish or vary very rapidly. This happens at the classical turning point $Q(\bar{x}) = 0$ or when $Q(x)$ has a steep behavior. Therefore WKB approximation is in particular not valid in the vicinity of the classical turning point $\bar{x}$.

Application of the WKB approximation Let's go back to the equation of motion of the mode function A_+ given in Eq. (2.8) and use WKB approximation to determine the approximate solution. To do so, one can introduce the new variable x defined as $x \equiv -k\tau$. Using this definition of x, Eq. (2.8) reads:

$$\frac{d^2A_+(x)}{dx^2} + \left(1 - \frac{2}{x}\frac{2\xi_*}{(x/x_*)^{\delta} + (x_*/x)^{\delta}}\right)A_+(x) = 0. \tag{2.23}$$

In order to cast the last equation in the form of Eq. (2.12) one can set, letting $\bar{x}$ unspecified:

$$1 - \frac{2}{x}\frac{2\xi_*}{(x/x_*)^{\delta} + (x_*/x)^{\delta}} \equiv Q(x) \equiv \begin{cases} p(x)^2 & , x > \bar{x} \\ -q(x)^2 & , x < \bar{x}, \end{cases} \tag{2.24}$$

where one can indeed recognise Eq. (2.12) with $\lambda = 1$. The solution for the mode function A_+ in terms of the functions p and q is then given in Eq. (2.19) and Eq. (2.22) with $\lambda = 1$ respectively in the regimes $x > \bar{x}$ and $x < \bar{x}$.
The next step is to fix some constants of integration using boundary conditions. The beginning of inflation corresponds to the limit $\tau \to -\infty$ or equivalently to the limit $x \to +\infty$ and so to scales deep in the horizon. A common assumption is to state that at such scales, the physics is the same as in flat Minkowski space-time where photons are in vacuum. This state is known as the Bunch-Davies vacuum and corresponds to the limit [27]:

$$\lim_{x\to+\infty} A_+(x) \stackrel{!}{=} \frac{1}{\sqrt{2k}} e^{ix} = \frac{1}{\sqrt{2k}}(\cos x + i \sin x). \tag{2.25}$$

$x > \bar{x}$: Bunch-Davies vacuum

In the context of WKB approximation for the mode function A_+, the Bunch-Davies vacuum corresponds to the regime $x > \bar{x}$ with $x \to +\infty$. Matching the solution for the mode function A_+ in the regime $x > \bar{x}$ given in Eq. (2.19) with the Bunch-Davies vacuum given in Eq. (2.25) leads to, with $\lim_{x\to+\infty} p(x) = 1$ and making the approximation $x - \bar{x} + \pi/4 \approx x$ when $x \to +\infty$, $\alpha_1 = 1/\sqrt{2k}$ and $\beta_1 = -i/\sqrt{2k}$.

Now that the solution for the mode function A_+ is determined in both regimes $x > \bar{x}$ and $x < \bar{x}$ with fixed constants α_1 and β_1, the next step is to connect the solutions $A_+(x > \bar{x})$ and $A_+(x < \bar{x})$ in the vicinity of the classical turning point $\bar{x}$ where WKB approximation does not hold. In the vicinity of $\bar{x}$, the equation of motion of the mode function A_+ given in Eq. (2.23) can be approximated as:

$$A_+''(x) + Q'(\bar{x})(x - \bar{x})A_+(x) = 0. \tag{2.26}$$

In order to cast the last equation into the form of the well-known Airy equation, one can introduce the new variable $z \equiv [-Q'(\bar{x})]^{1/3}(x - \bar{x})$ and set $A(x) \equiv y(z(x))$ which will simply be denoted $y(z)$ from now on. With these definitions, Eq. (2.26) indeed takes the form of the Airy equation such that the solution is given by $y(z) = d_1\,\mathrm{Ai}(z) + d_2\,\mathrm{Bi}(z)$ with $d_{1,2}$ some constants to be determined, $\mathrm{Ai}(z)$ the Airy function of first kind and $\mathrm{Bi}(z)$ the Airy function of second kind.
The final step is to match the solution $y(z) = d_1\,\mathrm{Ai}(z) + d_2\,\mathrm{Bi}(z)$ that holds in the vicinity of $\bar{x}$ to the solutions obtained with WKB approximation in the regimes $x > \bar{x}$ and $x < \bar{x}$.

$x > \bar{x}$: Matching the solution from WKB approximation with the solution in the vicinity of $\bar{x}$

The aim of this paragraph is to extend the solution $y(z)$ that holds in the vicinity of $\bar{x}$ to $x \to +\infty$, extend the solution obtained via WKB approximation that holds for $x > \bar{x}$ to the vicinity of $\bar{x}$ and match the two solutions.
The regime $x \to +\infty$, $x > \bar{x}$ corresponds to $z < 0 \Rightarrow \mathrm{Arg}\, z = \pi$. Then, in order to extend the solution $y(z)$ to $x \to +\infty$, one can use the asymptotic forms of Airy functions $\mathrm{Ai}(-z)$ and $\mathrm{Bi}(-z)$ for fixed $\mathrm{Arg}\, z$ such that $|\mathrm{Arg}\, z| < 2\pi/3$ when $|z| \to \infty$. Using only the leading term of the asymptotic forms of Airy functions, the solution of the Airy equation can be approximated as:

$$y(z) = d_1 \frac{1}{\sqrt{\pi} z^{1/4}} \sin\left(\frac{2}{3}(-z)^{3/2} + \frac{\pi}{4}\right) + d_2 \frac{1}{\sqrt{\pi} z^{1/4}} \cos\left(\frac{2}{3}(-z)^{3/2} + \frac{\pi}{4}\right). \tag{2.27}$$

On the other hand, in the vicinity of $\bar{x}$, $p(x) = \sqrt{Q'(\bar{x})(x - \bar{x})}$. Then the solution of the mode A_+ obtained via WKB approximation reads, in the vicinity of $\bar{x}$ and using the definition of z as a function of x:

$$A_+(z) = \frac{1}{z^{1/4}\sqrt{2k}[Q'(\bar{x})]^{1/6}} \cos\left(\frac{2}{3}(-z)^{3/2} + \frac{\pi}{4}\right) + \frac{i}{z^{1/4}\sqrt{2k}[Q'(\bar{x})]^{1/6}} \sin\left(\frac{2}{3}(-z)^{3/2} + \frac{\pi}{4}\right). \tag{2.28}$$

Matching Eq. (2.27) and Eq. (2.28) yields $d_1 = \sqrt{\frac{\pi}{2k}} \frac{i}{[Q'(\bar{x})]^{1/6}}$ and $d_2 = \sqrt{\frac{\pi}{2k}} \frac{1}{[Q'(\bar{x})]^{1/6}}$.

$x < \bar{x}$: Matching the solution from WKB approximation with the solution in the vicinity of $\bar{x}$

The aim of this paragraph is to extend the solution $y(z)$ that holds in the vicinity of $\bar{x}$ to $x \to -\infty$, extend the solution obtained via WKB approximation that holds for $x < \bar{x}$ to the vicinity of $\bar{x}$ and match the two solutions. The aim is to determine the coefficients α_2 and β_2 using the coefficients d_1 and d_2 obtained previously.
The regime $x \to -\infty$, $x < \bar{x}$ corresponds to $z > 0 \Rightarrow \mathrm{Arg}\, z = 0$. Then, in order to extend the solution $y(z)$ to $x \to -\infty$, one can use the asymptotic forms of Airy functions $\mathrm{Ai}(z)$ and $\mathrm{Bi}(z)$ for fixed $\mathrm{Arg}\, z$ such that $|\mathrm{Arg}\, z| < \pi$ when $|z| \to \infty$. Using only the leading term of the asymptotic forms of Airy functions, the solution of the Airy equation can be approximated as, using the explicit form of the coefficients d_1 and d_2:

$$y(z) = \frac{i}{2\sqrt{2k}[Q'(\bar{x})]^{1/6}} \frac{1}{z^{1/4}} \exp\left(-\frac{2}{3}z^{3/2}\right) + \frac{1}{\sqrt{2k}[Q'(\bar{x})]^{1/6}} \frac{1}{z^{1/4}} \exp\left(\frac{2}{3}z^{3/2}\right). \tag{2.29}$$

On the other hand, in the vicinity of $\bar{x}$, $q(x) = \sqrt{Q'(\bar{x})(x-\bar{x})}$. Then the solution of the mode A_+ obtained via WKB approximation reads, in the vicinity of $\bar{x}$ and using the definition of z:

$$A_+(z) = \frac{\alpha_2}{z^{1/4}[Q'(\bar{x})]^{1/6}} \exp\left(-\frac{2}{3}z^{3/2}\right) - \frac{\beta_2}{z^{1/4}[Q'(\bar{x})]^{1/6}} \exp\left(\frac{2}{3}z^{3/2}\right). \tag{2.30}$$

Matching Eq. (2.29) and Eq. (2.30) yields $\alpha_2 = \dfrac{i}{2\sqrt{2k}}$ and $\beta_2 = -\dfrac{1}{\sqrt{2k}}$.

Putting everything together, one can conclude that in the regime $x > \bar{x}$ the solution for the mode function A_+ is oscillating whereas in the regime $x < \bar{x}$ the solution is the sum of two exponential modes, with one growing mode. Therefore, the region of interest for this project is the region of exponential growth of the mode A_+ given by $x < \bar{x}$. In that region, it is then possible to make the approximation, keeping only the growing term and going back to the initial variable x:

$$A_+(x) = -\frac{1}{\sqrt{2kq(x)}} \exp\left(\int_x^{\bar{x}} q(x')dx'\right),\ x < \bar{x}. \tag{2.31}$$

It is important to stress here that Eq. (2.31) is valid for any $x < \bar{x}$. For now on, if not specified, the regime is the $x < \bar{x}$ regime.
The integral of the function q can not be computed exactly. However, one can note that:

$$\int_x^{\bar{x}} q(x')dx' = \int_0^{\bar{x}} q(x')dx' - \int_0^{x} q(x')dx'. \tag{2.32}$$

As the regime of interest is of moderately small x[3], it is possible to keep only the leading term in the function q as $x \to 0$ leading to:

$$\int_0^x q(x')dx' \approx \int_0^x \sqrt{\frac{4\xi_*}{x'(x'/x_*)^\delta}}dx' = \frac{4\sqrt{\xi_*}}{1+\delta}\left(\frac{x}{x_*}\right)^{\delta/2}\sqrt{x}. \tag{2.33}$$

Defining the scale dependent normalization factor N as:

$$N[x_*, \xi_*, \delta] \equiv \exp\int_0^{\bar{x}} q(x)dx, \tag{2.34}$$

this leads to, using $x \equiv -k\tau$:

$$A_+(\tau, k) = N[x_*, \xi_*, \delta]\left(\frac{-\tau}{8k\xi(\tau)}\right)^{1/4} \exp\left(-\frac{4\sqrt{\xi_*}}{1+\delta}\left(\frac{\tau}{\tau_*}\right)^{\delta/2}\sqrt{-k\tau}\right) \equiv \left(\frac{-\tau}{8k\xi(\tau)}\right)^{1/4}\tilde{A}(\tau, k). \tag{2.35}$$

The common way in literature to determine the normalization factor N is to solve the equation of motion of the mode function A_+ given in Eq. (2.8) numerically for fixed values of the parameters ξ_* and δ on a grid of x_*. Then the normalization factor N is obtained by matching the numerical solution with the WKB solution given in Eq. (2.35). A common practice in literature is to cast the normalization factor N into a log-normal form as:

$$N[x_*, \xi_*, \delta] = M\left[\xi_*, \delta\right] \exp\left(-\frac{1}{2\sigma^2[\xi_*, \delta]} \ln^2\left(\frac{x_*}{x[\xi_*, \delta]}\right)\right). \tag{2.36}$$

This has been done for instance in [34] and the log-normal form of the normalization factor N in an inflationary axion-$U(1)$ spectator model for fixed values of the parameter δ as a function of the parameter ξ_* is thus tabulated in literature. It is given by, for the two values of reference for the parameter δ [34]:

$$N[x_*, \xi_*, \delta] = \begin{cases} \exp\left[0.437 + 2.97\xi_* + 0.00105\xi_*^2\right] \exp\left(-\frac{1}{2[2.78-0.387\xi_*+0.0229\xi_*^2]^2} \ln^2\left(\frac{x_*}{-0.15+0.594\xi_*-0.00105\xi_*^2}\right)\right),\ \delta = 0.2 \\ \exp\left[0.117 + 2.54\xi_* + 0.000525\xi_*^2\right] \exp\left(-\frac{1}{2[1.51+0.22\xi_*+0.0137\xi_*^2]^2} \ln^2\left(\frac{x_*}{-0.05+0.683\xi_*-0.000716\xi_*^2}\right)\right),\ \delta = 0.5. \end{cases} \tag{2.37}$$

The solution of the gauge field operator $\vec{\hat{A}}$ is finally given by:

$$\hat{A}_i(\tau, \vec{x}) = \int \frac{d^3k}{(2\pi)^{3/2}} e^{i\vec{k}\cdot\vec{x}} A_+(\tau, k)\left[\epsilon_i^+(\hat{k})\hat{a}_+(\vec{k}) + \epsilon_i^{+*}(-\hat{k})\hat{a}_+^\dagger(-\vec{k})\right], \tag{2.38}$$

[3] Tachyonic instability occurs at large scales which translates into small wavenumber k and thus small x

with the mode function A_+ given in Eq. (2.35). From the solution of the gauge field operator $\hat{\vec{A}}$, two field operators, namely the "electric" and "magnetic" field operators $\hat{\vec{E}}$ and $\hat{\vec{B}}$, can be defined as:

$$\hat{E}_i(\tau,\vec{x}) \equiv -\frac{1}{a^2(\tau)}\hat{A}_i'(\tau,\vec{x}), \quad \hat{B}_i(\tau,\vec{x}) \equiv \frac{1}{a^2(\tau)}\epsilon_{ijk}\partial_j\hat{A}_k(\tau,\vec{x}). \tag{2.39}$$

To sum up, in this part, it has been shown that the mode function A_+ is indeed exponentially amplified. More in details, if the gauge field $\vec{A}$ is decomposed into two circular polarization modes $\hat{A}_\pm$, because the axion σ has a non-zero velocity its coupling to the gauge field $\vec{A}$ leads to the exponential growth of the mode A_+. This happens in the specific regime $x < \bar{x}$ at large scales, which is the regime in which the mode function A_+ gets a tachyonic mass term. As already pointed out, this exponential amplification of one polarization of the gauge field $\vec{A}$ can be interpreted as the production of quanta of the gauge field of plus polarization. The next sections are dedicated to the study of the phenomena that are due to the exponential production of quanta of the gauge field.

3 Sourced primordial tensor perturbations

The coupling between an axion and a $U(1)$ gauge field leads to an explosive production of quanta of the gauge field, as it has been shown in the previous section. This leads in turn to the production of scalar and tensor perturbations of the metric, shortly called scalar and tensor perturbations. This work focuses only on tensor perturbations and the aim of this section is to derive the equations, following [18], that highlight the fact that the explosive production of quanta of the gauge field indeed sources tensor perturbations and thus GWs.

3.1 Dynamics of the sourced tensor perturbations

Let introduce the transverse traceless tensor perturbations operator $\hat{h}_{ij}$, shortly called the tensor perturbations in the following, of the metric such that the metric takes the form:

$$ds^2 = a^2(\tau)\left[-d\tau^2 + (\delta_{ij} + \hat{h}_{ij}(\tau,\vec{x}))dx^i dx^j\right], \quad |\hat{h}_{ij}(\tau,\vec{x}))| \ll 1. \tag{3.1}$$

The aim of this section is to perform a calculation in perturbation theory [4], to expand the Lagrangian corresponding to the action given in Eq. (2.1) in powers of $\hat{h}_{ij}^2$ and derive the equation of motion of the tensor perturbations $\hat{h}_{ij}$.
The sourced term in the equation of motion of the tensor perturbations $\hat{h}_{ij}$ comes from the term $(1/4)F_{\mu\nu}F^{\mu\nu}$ (see the action given in Eq. (2.1)) which results into contributions of order one and two in the tensor perturbations $\hat{h}_{ij}$. Therefore, the contribution of order two in the tensor perturbations $\hat{h}_{ij}$ can be neglected in the sourced term compared to the contribution of order one. The remaining Lagrangian, denoted $\mathcal{L}_{\rm GW}$, then reads:

$$\mathcal{L}_{\rm GW} = \frac{M_P^2 a^2(\tau)}{8}[\hat{h}_{ij}'\hat{h}_{ij}'(\tau,\vec{x}) - \partial_k\hat{h}_{ij}(\tau,\vec{x})\partial_k\hat{h}_{ij}(\tau,\vec{x})] - \frac{a^4(\tau)}{2}\hat{h}_{ij}(\tau,\vec{x})[\hat{E}_i(\tau,\vec{x})\hat{E}_j(\tau,\vec{x}) + \hat{B}_i(\tau,\vec{x})\hat{B}_j(\tau,\vec{x})], \tag{3.2}$$

with $\hat{\vec{E}}$ and $\hat{\vec{B}}$ the "electric" and "magnetic" field operators defined in Eq. (2.39). Varying the action that corresponds to the Lagrangian $\mathcal{L}_{\rm GW}$ given in Eq. (3.2) with respect to the tensor perturbations $\hat{h}_{ij}$ and equating it to zero yields the equation of motion of the tensor perturbations $\hat{h}_{ij}$, using the explicit form of the scale factor $a(\tau) = -1/(H\tau)$:

$$\frac{M_P^2}{\tau}\hat{h}_{ij}'(\tau,\vec{x}) - \frac{M_P^2}{2}\hat{h}_{ij}''(\tau,\vec{x}) + \frac{M_P^2}{2}\partial_k^2\hat{h}_{ij}(\tau,\vec{x}) - \frac{1}{H^2}[\hat{E}_i(\tau,\vec{x})\hat{E}_j(\tau,\vec{x}) + \hat{B}_i(\tau,\vec{x})\hat{B}_j(\tau,\vec{x})] = 0. \tag{3.3}$$

One can quantize the tensor perturbations $\hat{h}_{ij}$ using the definition:

$$\hat{h}_{ij}(\tau,\vec{x}) = \sum_{\lambda=\pm}\int\frac{d^3k}{(2\pi)^{3/2}}e^{i\vec{k}\cdot\vec{x}}\Pi_{ij,\lambda}^*(\hat{k})\hat{h}_\lambda(\tau,\vec{k}) \equiv \frac{2}{M_P a(\tau)}\sum_{\lambda=\pm}\int\frac{d^3k}{(2\pi)^{3/2}}e^{i\vec{k}\cdot\vec{x}}\Pi_{ij,\lambda}^*(\hat{k})\left[h_\lambda(\tau,k)\hat{b}_\lambda(\vec{k}) + \text{h.c.}\right], \tag{3.4}$$

where $\lambda = \pm$ denotes the polarization, $\hat{h}_\lambda(\tau,\vec{k})$ is the tensor mode operator associated to the tensor perturbations operator $\hat{h}_{ij}$, $h_\lambda(\tau,\vec{k})$ is the mode function associated to the tensor perturbations operator $\hat{h}_{ij}$, $\Pi_{ij,\lambda}^*(\hat{k}) \equiv \epsilon_i^\lambda(\hat{k})\epsilon_j^\lambda(\hat{k})$ is the polarization tensor with $\vec{\epsilon}^\lambda(\hat{k})$ the same polarization vector as in the previous section thus satisfying the same properties given in Eq. (2.10) and $\hat{b}_\lambda^\dagger(\vec{k})$, $\hat{b}_\lambda(\vec{k})$ are respectively the creation and annihilation operators associated to the tensor perturbations $\hat{h}_{ij}$ satisfying the commutation relation $[\hat{b}_\lambda(\vec{k}), \hat{b}_{\lambda'}^\dagger(\vec{p})] = \delta_{\lambda\lambda'}\delta^{(3)}(\vec{k}-\vec{p})$.

[4] This is possible as the assumption $|\hat{h}_{ij}(\tau,\vec{x}))| \ll 1$ means that the tensor perturbations of the metric are considered being small perturbations on top of the metric.

Using the definition given in Eq. (3.4), the equation of motion of the tensor mode operator $\hat{h}_\lambda$ reads:

$$\left(\frac{\partial^2}{\partial\tau^2}+k^2-\frac{2}{\tau^2}\right)\left(\frac{M_P a(\tau)}{2}\hat{h}_\lambda(\tau,\vec{k})\right)=-\frac{a^3(\tau)}{M_P}\Pi_{ij,\lambda}(\hat{k})\int\frac{d^3x}{(2\pi)^{3/2}}e^{-i\vec{k}\vec{x}}[\hat{E}_i(\tau,\vec{x})\hat{E}_j(\tau,\vec{x})+\hat{B}_i(\tau,\vec{x})\hat{B}_j(\tau,\vec{x})]\equiv\hat{S}_\lambda(\tau,\vec{k}). \tag{3.5}$$

The equation Eq. (3.5) can be understood as follows. The gradients of the gauge field $\vec{A}$ given by the "electric" and "magnetic" fields $\vec{E}$ and $\vec{B}$ (see Eq. (2.39)) act as a source of tensor perturbations of the metric. As the gauge field $\vec{A}$ is exponentially amplified, its gradients are non-zero and source tensor perturbations of the metric i.e. GWs according to Eq. (3.5).
The solution for the tensor mode operator $\hat{h}_\lambda$ is obtained by separating it into two contributions: $\hat{h}_\lambda=\hat{h}_\lambda^{(0)}+\hat{h}_\lambda^{(1)}$. The contribution labelled with (0) is the homogeneous solution of Eq. (3.5) obtained by equating the right-hand-side of Eq. (3.5) to zero. This contribution is called the vacuum contribution because it corresponds to the contribution of the vacuum fluctuations. The contribution labelled with (1) corresponds to a particular solution of Eq. (3.5) called the sourced contribution because it is sourced by the gradients of the gauge field $\vec{A}$. One can assume that the vacuum and sourced contributions are statistically uncorrelated.

The vacuum contribution to $\hat{h}_\lambda$ The vacuum contribution $\hat{h}_\lambda^{(0)}$ of the tensor mode operator $\hat{h}_\lambda$ satisfies Eq. (3.5) with zero right-hand-side. The corresponding vacuum contribution to the mode function $h_\lambda^{(0)}$ thus satisfies the so-called Mukhanov-Sasaki equation [22, 23]:

$$\left(\frac{\partial^2}{\partial\tau^2}+k^2-\frac{2}{\tau^2}\right)h_\lambda^{(0)}(\tau,k)=0. \tag{3.6}$$

Assuming that the mode function $h_\lambda^{(0)}$ satisfies Bunch-Davies boundary conditions (given in Eq. (2.25)), the solution of Eq. (3.6) is given by [27]:

$$h_\lambda^{(0)}(\tau,k)=\frac{1}{\sqrt{2k}}\left(1-\frac{i}{k\tau}\right)\mathrm{e}^{-ik\tau}\Rightarrow\hat{h}_\lambda(\tau,\vec{k})=\frac{2}{M_P a(\tau)}\frac{1}{\sqrt{2k}}\left[\left(1-\frac{i}{k\tau}\right)\mathrm{e}^{-ik\tau}\hat{b}_\lambda(\vec{k})+\left(1+\frac{i}{k\tau}\right)\mathrm{e}^{ik\tau}\hat{b}_\lambda^\dagger(-\vec{k})\right]. \tag{3.7}$$

The sourced contribution to $\hat{h}_\lambda$ The sourced contribution $\hat{h}_\lambda^{(1)}$ to the tensor mode operator $\hat{h}_\lambda$ satisfies Eq. (3.5) and can therefore be formally solved using the retarded Green function $G_k(\tau,\tau')$ associated to the operator $(\partial^2/\partial\tau^2)+k^2-2/\tau^2$. The function DSolve from Mathematica gives the retarded Green function:

$$G_k(\tau,\tau')=\Theta(\tau-\tau')\frac{\pi}{2}\sqrt{\tau\tau'}[J_{3/2}(-k\tau)Y_{3/2}(-k\tau')-Y_{3/2}(-k\tau)J_{3/2}(-k\tau')], \tag{3.8}$$

where the function $\Theta(\tau-\tau')$ stands for the retarded Green function i.e. the Green function is non-zero only if $\tau'\leq\tau$ and $J(-k\tau)$, $Y(-k\tau)$ are respectively the Bessel functions of first and second kind of real argument. The sourced contribution $\hat{h}_\lambda^{(1)}$ to the tensor mode operator is thus given by:

$$\hat{h}_\lambda^{(1)}(\tau,\vec{k})=\frac{2}{M_P a(\tau)}\int^\tau d\tau' G_k(\tau,\tau')\hat{S}_\lambda(\tau',\vec{k}). \tag{3.9}$$

In the regime of interest of this work, which is at large scales or equivalently for $-k\tau\ll1$, the retarded Green function G_k can be approximated by, using the asymptotic forms of the Bessel functions as well as the explicit form of the Bessel function of first kind $J_{3/2}(z)$:

$$G_k(\tau,\tau')=\frac{\Theta(\tau-\tau')}{k^3\tau\tau'}\left(-\sin(k\tau')+\cos(k\tau')k\tau'\right),\ -k\tau\ll1. \tag{3.10}$$

In addition, the source mode function $\hat{S}_\lambda(\tau,\vec{k})$ can be explicitly written as:

$$\begin{aligned}\hat{S}_\lambda(\tau,\vec{k})=&-\frac{H}{M_P}\sqrt{\frac{\tau\xi(\tau)}{2}}\Pi_{ij,\lambda}(\hat{k})\int\frac{d^3p}{(2\pi)^{3/2}}p^{1/4}|\vec{k}-\vec{p}|^{1/4}\left(1+\frac{\sqrt{p|\vec{k}-\vec{p}|}\tau}{2\xi(\tau)}\right)\tilde{A}(\tau,p)\tilde{A}(\tau,|\vec{k}-\vec{p}|)\\&\cdot\left[\epsilon_i^+(\hat{p})\hat{a}_+(\vec{p})+\epsilon_i^{+*}(-\hat{p})\hat{a}_+^\dagger(-\vec{p})\right]\left[\epsilon_j^+(\hat{k}-\hat{p})\hat{a}_+(\vec{k}-\vec{p})+\epsilon_j^{+*}(-\hat{k}+\hat{p})\hat{a}_+^\dagger(-\vec{k}+\vec{p})\right].\end{aligned} \tag{3.11}$$

At large scales, the sourced contribution $\hat{h}_\lambda^{(1)}$ to the tensor mode operator is then given by [5]:

$$\begin{aligned}\hat{h}_\lambda^{(1)}(\tau,\vec{k})=&\frac{\sqrt{2}H^2}{M_p^2k^{7/2}}\Pi_{ij,\lambda}(\hat{k})\int\frac{d^3p}{(2\pi)^{3/2}}p^{1/4}|\vec{k}-\vec{p}|^{1/4}\\&\cdot N\left[\frac{p}{k_*},\xi_*,\delta\right]N\left[\frac{|\vec{k}-\vec{p}|}{k_*},\xi_*,\delta\right]T\left[x_*,\xi_*,\delta,\frac{p}{k},\frac{|\vec{k}-\vec{p}|}{k}\right]\\&\cdot\left[\epsilon_i^+(\hat{p})\hat{a}_+(\vec{p})+\epsilon_i^{+*}(-\hat{p})\hat{a}_+^\dagger(-\vec{p})\right]\left[\epsilon_j^+(\hat{k}-\hat{p})\hat{a}_+(\vec{k}-\vec{p})+\epsilon_j^{+*}(-\hat{k}+\hat{p})\hat{a}_+^\dagger(-\vec{k}+\vec{p})\right],\end{aligned} \tag{3.12}$$

[5] The fact that the vacuum and the sourced contributions do not depend on the same creation and annihilation operators can be surprising at first sight. It is however consistent because the two contributions are uncorrelated and therefore not created via the same mechanism.

where the function T is defined as:

$$T\left[x_*,\xi_*,\delta,p,q\right] \equiv \int_0^\infty dx' \left(x'\cos x' - \sin x'\right)\sqrt{\frac{\xi\left(x'\right)}{x'}}\exp\left[-\frac{4\xi_*^{1/2}}{1+\delta}\frac{x'^{(1+\delta)/2}}{x_*^{\delta/2}}(\sqrt{p}+\sqrt{q})\right] + \frac{\sqrt{pq}}{2}\int_0^\infty dx' \left(x'\cos x' - \sin x'\right)\sqrt{\frac{x'}{\xi\left(x'\right)}}\exp\left[-\frac{4\xi_*^{1/2}}{1+\delta}\frac{x'^{(1+\delta)/2}}{x_*^{\delta/2}}(\sqrt{p}+\sqrt{q})\right], \tag{3.13}$$

with $x' \equiv -k\tau'$.
To sum, it has been shown in this part that the gradients of the gauge field $\vec{A}$ source tensor perturbations of the metric. These tensor perturbations have two uncorrelated contributions: the standard vacuum contribution from inflation and a contribution sourced by the coupling between the axion σ and the gauge field $\vec{A}$. Both these contributions are stretched to cosmological scales due to the exponential expansion of the universe, leave the horizon and freeze out. They re-enter the observable universe during the reheating stage after inflation as GWs that carry information about inflation and the specific inflationary axion-$U(1)$ spectator model. This is the scenario presented in the Introduction.

3.2 Tensor power spectrum

The observable associated to perturbations is the power spectrum. This section is therefore dedicated to the derivation of the tensor power spectrum which is the observable associated to the tensor perturbations.
The tensor power spectrum $\mathcal{P}_\lambda$ associated to the tensor perturbations is related to the correlator at equal times of the tensor mode operator $\hat{h}_\lambda$ associated to the tensor perturbations operator via the definition:

$$\mathcal{P}_\lambda(k)\delta_{\lambda\lambda'}\delta^{(3)}(\vec{k}+\vec{k'}) \equiv \frac{k^3}{2\pi^2}\langle 0|\hat{h}_\lambda(\tau,\vec{k})\hat{h}_{\lambda'}(\tau,\vec{k'})|0\rangle, \tag{3.14}$$

where $|0\rangle$ denotes the quantum vacuum state of the system. As the tensor mode operator $\hat{h}_\lambda$ consists in two uncorrelated contributions, the tensor power spectrum thus consists in two uncorrelated contributions, a vacuum contribution $\mathcal{P}_\lambda^{(0)}$ that depends only on the vacuum contribution $\hat{h}_\lambda^{(0)}$ of the tensor mode operator associated to the tensor perturbations and a sourced contribution $\mathcal{P}_\lambda^{(1)}$ that depends only on the sourced contribution $\hat{h}_\lambda^{(1)}$ of the tensor mode operator.

The vacuum contribution to the tensor power spectrum At large scales, the vacuum contribution to the tensor power spectrum is given by:

$$\mathcal{P}_\lambda^{(0)}(k)\delta_{\lambda\lambda'}\delta^{(3)}(\vec{k}+\vec{k'}) = \frac{k^3}{2\pi^2}\langle 0|\hat{h}_\lambda^{(0)}(\tau,\vec{k})\hat{h}_{\lambda'}^{(0)}(\tau,\vec{k'})|0\rangle \Rightarrow \mathcal{P}_\lambda^{(0)} = \frac{H^2}{\pi^2 M_P^2}, \tag{3.15}$$

which is the standard result known from simple models of inflation without any additional particle production [4].

The sourced contribution to the tensor power spectrum The sourced contribution to the tensor power spectrum $\mathcal{P}_\lambda^{(1)}$ is derived "brute force", giving (see Appendix A for more details):

$$\mathcal{P}_\lambda^{(1)}(k) = \left(\frac{H^2}{M_P^2}\right)^2 \frac{1}{8\pi^2}\int\frac{d^3q}{(2\pi)^3}(1+\lambda\hat{k}\cdot\hat{q})^2\left(1+\lambda\hat{k}\cdot\frac{\vec{k}-\vec{q}}{|\vec{k}-\vec{q}|}\right)\sqrt{q|\vec{k}-\vec{q}|} \cdot N^2\left[qx_*,\xi_*,\delta\right]N^2\left[|\vec{k}-\vec{q}|x_*,\xi_*,\delta\right]T\left[x_*,\xi_*,\delta,q,|\vec{k}-\vec{q}|\right]. \tag{3.16}$$

The change of variables $u \equiv q + |\vec{k}-\vec{q}|$, $v \equiv q - |\vec{k}-\vec{q}|$ leads to:

$$\mathcal{P}_\lambda^{(1)}(k) = \left(\frac{H^2}{8\pi^2 M_P^2}\right)^2 p_\lambda(x_*,\xi_*,\delta),$$
$$p_\lambda(x_*,\xi_*,\delta) = \frac{1}{4}\int_1^\infty du\int_0^1 dv\frac{(1-v^2)^2(1+\lambda u^2)^2}{\sqrt{u^2-v^2}}N^2\left[\frac{u+v}{2}x_*,\xi_*,\delta\right]N^2\left[\frac{u-v}{2}x_*,\xi_*,\delta\right]T\left[x_*,\xi_*,\delta,\frac{u+v}{2},\frac{u-v}{2}\right]. \tag{3.17}$$

The function p_λ can not be computed analytically. The common procedure in literature is to solve p_λ numerically using the solution for gauge field operator $\vec{\hat{A}}$ given in Eq. (2.38) that depends on the mode function A_+ and to cast p_λ into a log-normal form:

$$p_\lambda(x,\xi_*,\delta) = M_\lambda\left[\xi_*,\delta\right]\exp\left(-\frac{1}{2\sigma_\lambda^2[\xi_*,\delta]}\ln^2\left(\frac{x}{x_\lambda[\xi_*,\delta]}\right)\right). \tag{3.18}$$

(λ, δ)	$\ln\lvert M_\lambda[\xi_*, \delta]\rvert$	$\sigma_\lambda[\xi_*, \delta]$	$x_\lambda[\xi_*, \delta]$
$(+, 0.2)$	$-7.98 + 10\xi_* + 0.0979\xi_*^2$	$1.38 - 0.178\xi_* + 0.0103\xi_*^2$	$5.45 + 0.455\xi_* + 0.0316\xi_*^2$
$(-, 0.2)$	$-13.8 + 9.96\xi_* + 0.104\xi_*^2$	$1.44 - 0.169\xi_* + 0.0102\xi_*^2$	$2.39 + 0.129\xi_* + 0.0214\xi_*^2$
$(+, 0.5)$	$-6.85 + 9.05\xi_* + 0.0596\xi_*^2$	$0.768 - 0.00993\xi_* + 0.00608\xi_*^2$	$2.7 + 0.896\xi_* + 0.0187\xi_*^2$
$(-, 0.5)$	$-12.5 + 8.97\xi_* + 0.0656\xi_*^2$	$0.858 - 0.0813\xi_* + 0.0053\xi_*^2$	$1.22 + 0.396\xi_* + 0.00976\xi_*^2$

Table 1: Tabulated ξ_* dependence of the functions entering in Eq. (3.18) for polarizations $\lambda = \pm$ and two fixed values $\delta = 0.2, 0.5$ [18]

The log-normal form of the function p_λ for an inflationary axion-$U(1)$ spectator model is tabulated for fixed values of the parameter δ [6]. It is given Tab.1 for the two reference values of the parameter δ. From Tab.1, for $\delta = 0.2$ the function p_- is suppressed compared to the function p_+ by a relative factor $e^{-7.98+13.8} \approx 340$ and for $\delta = 0.5$ the function p_- is suppressed by a relative factor $e^{-6.85+12.5} \approx 280$. The function p_- can therefore be safely neglected in the following sections and the label λ will be dropped.
The total tensor power spectrum $\mathcal{P}$ is finally given by, noting that $x_* = k/k_*$:

$$\mathcal{P}(k) = \frac{H^2}{\pi^2 M_P^2}\left[1 + \frac{H^2}{64\pi^2 M_P^2} p\left(\frac{k}{k_*}, \xi_*, \delta\right)\right], \tag{3.19}$$

where, as already pointed out, the function p stands for the log-normal form of the function p_+ defined in Eq. (3.18).
The result obtained for the function p_λ, namely $p_- \ll p_+$ is not trivial and has actually important phenomenological consequences. As the function p_λ describes completely the tensor power spectrum, $p_- \ll p_+$ implies that $\mathcal{P}_- \ll \mathcal{P}_+$. This means that the GWs produced by the inflationary axion-$U(1)$ spectator model are highly chiral. As the derivation presented in this work is completely model-dependent, the results can lead to the conclusion that a chiral GW spectrum is the signature of an inflationary model with the presence of a spectator rolling axion coupled to a $U(1)$ gauge field.

3.3 Constraints of the low-backreaction regime

The derivation of the contribution p_λ to the total tensor power spectrum lies in the low-backreaction regime where the plus polarization of the gauge field $\vec{A}$ is exponentially amplified and where backreactions of the gauge field $\vec{A}$ onto the axion dynamics are negligible. The aim of this section is to determine the bounds of the low-backreaction regime that will be the domain of validity of this work. More precisely, the aim is to derive a constraint on the parameters ξ_* and δ following the reasoning of [24, 25].
As already mentioned Sec.2.1, because the axion σ is considered spectator i.e. because inflation is assumed being driven by the inflaton ϕ, the contribution of the axion energy density to the total energy density is negligible compared to the contribution of the inflaton energy density. This assumption translates into $\rho_\sigma \ll \rho_\phi \approx V(\phi) \approx 3H^2 M_P^2$. In addition, because the axion σ is assumed being slowly rolling, its potential energy density dominates over its kinetic energy density so that $\rho_\sigma \approx V_\sigma$. These considerations lead to the constraint $V_\sigma \ll 3H^2 M_P^2$. Assuming that the axion σ starts its motion close to the maximum of its potential at $\sigma = 0$, the maximal value of the axion potential energy density is always smaller than $V_\sigma(0) = \Lambda^4$. Then, to ensure the constraint $V_\sigma \ll 3H^2 M_P^2$, one can set, using the definition of the parameter δ given in Eq. (2.5):

$$\max(V_\sigma) \ll 3H^2 M_P^2 \Rightarrow \frac{f}{M_P} \ll \frac{1}{\sqrt{2\delta}}, \tag{3.20}$$

where $\max(V_\sigma)$ denotes the maximal value of the axion potential energy density.
As also pointed out Sec.2.1, the fact that the backreaction of the gauge field $\vec{A}$ onto the axion dynamics is negligible translates into the condition $\rho_A \ll \rho_\sigma$. More precisely, as the gauge field $\vec{A}$ is amplified at the expense of the axion kinetic energy[7], to ensure that the production of quanta of the gauge field does not influence the axion dynamics, it is possible to impose that the maximum of the gauge field energy density must be smaller than the maximum of the axion kinetic energy density. This leads to the constraint, dropping the dependence on the conformal time τ:

$$\max(\rho_A) \ll \max\left(\frac{\dot{\sigma}}{2}\right) = \rho_\phi \frac{f^2\delta^2}{6M_P^2} \Rightarrow \frac{1}{\delta}\sqrt{\frac{6\max(\rho_A)}{\rho_\phi}} \ll \frac{f}{M_P}. \tag{3.21}$$

Putting together Eq. (3.20) and Eq. (3.21) gives a constraint on the maximal energy density of the gauge field compared to a quantity that depends only on the parameter δ. In order to derive a constraint on the parameters ξ_* and δ, one has to determine the maximal energy density of the gauge field as a function of the parameter ξ_*. This can be done explicitly for

[6] The function p_λ could have been computed numerically using the functions NIntegrate and FindNonLinearFit from Mathematica. Because of time constraints, it has been decided to take the result from literature.

[7] The coupling between the axion and the gauge field induces a friction term in the equation of motion of the axion. In the low-backreaction regime, this friction is negligible leading to the constraint on the energy density of the gauge field.

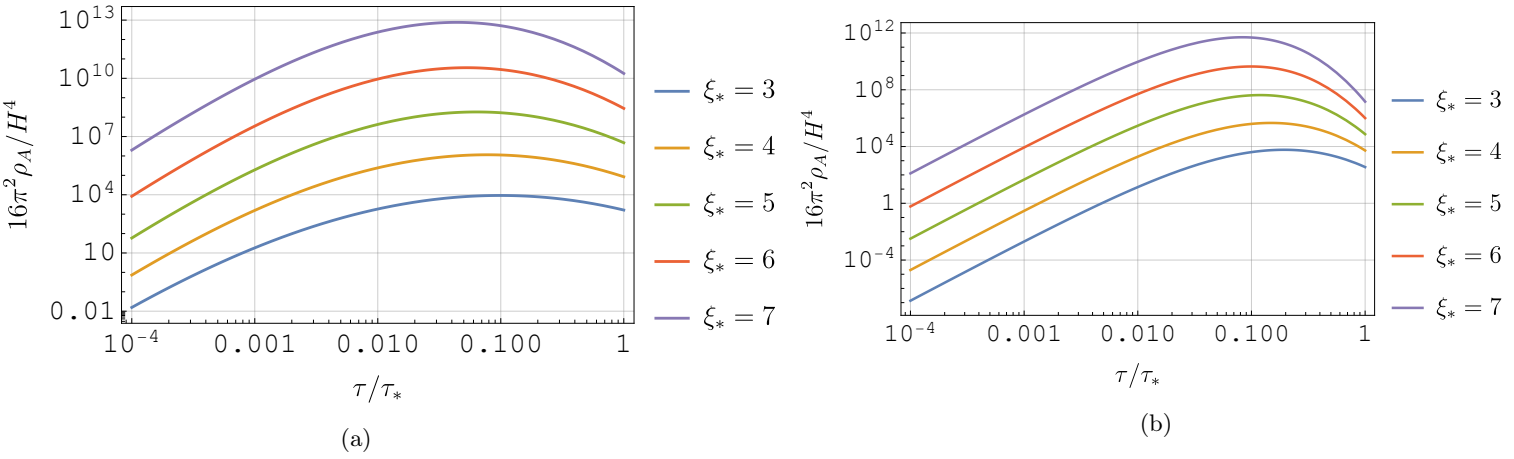

Figure 3: Total energy density in the gauge field $\vec{A}$ corresponding to the integral given in Eq. (3.24) computed numerically with the function NIntegrate from Mathematica for different values of the parameter ξ_* given in Eq. (2.7) and two different values of the parameter δ given in Eq. (2.5) (a) $\delta = 0.2$ (b) $\delta = 0.5$.

the two values of reference of the parameter δ, in order to get a constraint on the parameter ξ_* for each value of reference of the parameter δ. This is what is done in the following.
Analogously to electromagnetism, the energy density of the gauge field ρ_A can be defined as:

$$\rho_A(\tau) \equiv \frac{1}{2}\langle 0|\left(\vec{E}^2(\tau,\vec{x}) + \vec{B}^2(\tau,\vec{x})\right)|0\rangle, \tag{3.22}$$

with $\vec{E}$ and $\vec{B}$ the "electric" and "magnetic" field operators defined in Eq. (2.39). Using the explicit definitions of the "electric" and "magnetic" field operators, the energy density of the gauge field reads, in spherical coordinates:

$$\rho_A(\tau) = \frac{1}{4\pi^2 a^4(\tau)} \int dk \left[k^2 \left|A'_+(\tau,k)\right|^2 + k^4 \left|A_+(\tau,k)\right|^2\right]. \tag{3.23}$$

Using the variable $x \equiv -k\tau$ and the explicit form of the mode function A_+ given in Eq. (2.35) as well as the log-normal form of the normalization factor N given in Eq. (2.36), the energy density of the gauge field ρ_A takes the form:

$$\rho_A(\tau) = \frac{H^4}{16\pi^2} \frac{(\tau/\tau_*)^{7/2} M^2\left[\xi_*,\delta\right]}{\sqrt{\xi_*}\sqrt{(\tau/\tau_*)^{\delta} + (\tau/\tau_*)^{-\delta}}} \int_0^{\infty} dx_* x_*^{5/2} \exp\left[\frac{-8\sqrt{\xi_*}}{1+\delta}(\tau/\tau_*)^{\delta/2+1}\sqrt{x_*} - \frac{1}{\sigma^2\left[\xi_*,\delta\right]} \ln^2\left(\frac{x_*}{x[\xi_*,\delta]}\right)\right] \cdot \left[4\xi_* + x_*(\tau/\tau_*)\left((\tau/\tau_*)^{\delta} + (\tau/\tau_*)^{-\delta}\right)\right]. \tag{3.24}$$

For the two values of reference of the parameter δ, it is possible to solve the integral given in Eq. (3.24) numerically for different values of the parameter ξ_*. The results are given in Fig.3. From Fig.3 it appears that the energy density of the gauge field ρ_A presents a clear maximum for the chosen set of values of the parameter ξ_* and both values of the parameter δ at time $\tau/\tau_* \sim \mathcal{O}(0.1)$. Taking a set of values of the parameter ξ_*, it is possible to extract the maximal value of the energy density of the gauge field for each value of the parameter ξ_* using the function FindMaximum from Mathematica. Then, using the function NonLinearModelFit from Mathematica allows to determine a fit function at 95% confidence level for the maximal energy density of the gauge field as a function of the parameter ξ_*. This has been done for the two values of reference of the parameter δ and the result reads:

$$\frac{16\pi^2 \max\left(\rho_A\right)}{H^4} = \begin{cases} 6.7 \cdot 10^{-3} \exp\left[1.63\pi\xi_*\right], \ \delta = 0.2 \\ 2.8 \cdot 10^{-2} \exp\left[1.52\pi\xi_*\right], \ \delta = 0.5. \end{cases} \tag{3.25}$$

NB: *No uncertainty is given on the fit of the energy density of the gauge field. This is due to the fact that the expression of the energy density of the gauge field is an integral computed numerically and therefore it is not possible to quantify an uncertainty on the maximal value of the energy density of the gauge field and thus on the fit function.*

It is useful at this point to introduce the tensor-to-scalar ratio r defined as the ratio between the tensor power spectrum and the curvature power spectrum, and therefore to introduce the notion of curvature perturbations. In spatially flat gauge, which is the gauge chosen in this work, the curvature perturbations operator $\hat{\zeta}$ is related to the inflaton perturbation operator $\delta\hat{\phi}$ via the relation [4]:

$$\hat{\zeta}(\tau,\vec{k}) = -\frac{H}{\dot{\phi}(\tau)}\delta\hat{\phi}(\tau,\vec{k}). \tag{3.26}$$

It is possible to follow the same kind of reasoning as the one presented Sec.3 to derive the equation of motion of the inflaton perturbations operator $\delta\hat{\phi}$ that gives the curvature perturbations operator using Eq. (3.26). Then, the curvature power spectrum is defined in the same way as the tensor power spectrum i.e. is proportional to the correlator at equal time of the curvature perturbations operator. In an inflationary model where inflation is driven by a single inflaton ϕ, the vacuum contribution to the curvature power spectrum $\mathcal{P}_\zeta^{(0)}$ is well-known. It is a standard relation and it has also been measured [4, 26]:

$$\mathcal{P}_\zeta^{(0)} = \frac{H^2}{8\pi^2\epsilon_\phi M_P^2} = 2.1\cdot 10^{-9}, \tag{3.27}$$

where ϵ_ϕ is the inflaton slow-roll parameter defined as $\epsilon_\phi \equiv \dot{\phi}^2/(2M_P^2H^2)$. Using the result derived for the vacuum contribution to the tensor power spectrum given in Eq. (3.15), the vacuum contribution to the tensor-to-scalar ratio $r_{\rm vac}$, shortly called the vacuum tensor-to-scalar ratio, is given by:

$$r_{\rm vac} \equiv \frac{\mathcal{P}_\lambda^{(0)}}{\mathcal{P}_\zeta^{(0)}} = 16\epsilon_\phi \Rightarrow \frac{H^2}{M_P^2} = \left(2.1\cdot 10^{-9}\right)\frac{\pi^2}{2}r_{\rm vac}. \tag{3.28}$$

This last expression thus allows to express the Hubble rate H in terms of the vacuum tensor-to-scalar ratio $r_{\rm vac}$.
Going back to the energy density of the gauge field ρ_A and the constraints given in Eq. (3.20) and Eq. (3.21), putting everything together leads to the constraints on the parameter ξ_*:

$$\xi_* \ll \begin{cases} \dfrac{1}{0.815\pi}\ln\left[\dfrac{1.58}{4.69\cdot 10^{-6}\sqrt{r_{\rm vac}}}\right], \ \delta = 0.2 \\ \dfrac{1}{0.76\pi}\ln\left[\dfrac{1}{3.38\cdot 10^{-6}\sqrt{r_{\rm vac}}}\right], \ \delta = 0.5, \end{cases} \tag{3.29}$$

which is the domain of validity of this project in the parameter space $(r_{\rm vac}, \xi_*)$.

4 Data analysis

In the previous sections, the inflationary axion-$U(1)$ spectator model has been presented, the equations of motion of the fields and of the tensor perturbations derived and the corresponding tensor power spectrum computed. It has been shown that in the inflationary axion-$U(1)$ spectator model, the plus polarization of the gauge is exponentially amplified, leading to tensor perturbations of the metric that can be observed. This section is dedicated to the comparison of the analytical results obtained in the previous sections with the PTA data collected by the NANOGrav collaboration. The aim is to perform a Bayesian statistical analysis of the inflationary axion-$U(1)$ spectator model with the PTA data set collected by the NANOGrav collaboration. This inflationary model including several free parameters, the aim of the Bayesian statistical analysis is to derive constraints on the free parameters such that for values of the free parameters that satisfy the constraints, the GW spectrum produced could explain the PTA data.

4.1 Pulsar Timing Array data and PTArcade

This section aims to give an introductory presentation of PTA data and PTA data analysis. For more details, see [28].
Pulsars are a type of neutron star that result from stellar collapse. Pulsars are rapidly rotating and highly magnetized and can thus be viewed as rotating magnetized dipoles. They generate a local electric field along which charged particles are accelerated. These accelerated charged particles excite beams of radio emission that can be observed from Earth when the rotating beam intersects the Earth line-of-sight. This allows the measure of the pulse period which is a measure of the period of rotation of the pulsar. The period of rotation of pulsars being almost constant, they can be used as astrophysical tools as time-keepers. This is how pulsars are used to collect PTA data. More in detail, the measurement of PTA data follows several steps. Fist, several stable pulsars of period of rotation of milliseconds are chosen. Second, for each pulsar, a timing model is constructed. This timing model should predict the time of arrival of the pulsar pulse. It includes individual internal processes of the pulsar, white noise and internal processes that are common to all pulsars but uncorrelated. Then, each pulsar is observed over a time lapse, its pulse time of arrival is measured and the timing residual is estimated. This timing residual corresponds to the difference between the prediction of the timing model and the measured time of arrival. The timing residuals are thus generated by any phenomena that are not included in the timing model, which includes GWs. Indeed, if a GW passes through spacetime, it should stretch spacetime in one direction and squeeze it in the opposite direction, inducing redshifts of the pulse time of arrival that should be correlated among all pulsars. This kind of phenomenon is indeed not including in the timing model. The search for a GW spectrum consists in computing cross-correlations of timing residuals between pairs of pulsars. This cross-correlation can be written as the product of two factor: a power spectrum common to all pulsars and the overlap reduction function that measures how much GW spectrum is shared between pairs of pulsars. The first factor can be related to the characteristic GW spectrum and is therefore the quantity of interest. PTA data are thus the cross-correlations of timing residuals between pairs of pulsars as a function of frequency for all observed pulsars. The frequencies are separated into 30 bins of frequencies.

PTA data analysis uses Bayesian statistics. Therefore this analysis lies on Bayes' theorem, that reads, for a parameter θ and data d:

$$p(\theta|d) = \frac{p(d|\theta)p(\theta)}{p(d)}, \tag{4.1}$$

where p denotes the probability distribution, $p(\theta|d)$ is the posterior probability distribution of the parameter θ, $p(d|\theta)$ is the likelihood of the parameter θ, $p(\theta)$ is the prior probability distribution of the parameter θ and $p(d)$ is the evidence. Traditionally, processes that are common to all pulsars are assumed being sourced by SMBHBs. Therefore, the corresponding GW spectrum $\Omega_{\rm GW,\ SMBHB}$ is traditionally modelled by the simplest SMBHB GW spectrum, which is a power-law of the form [29]:

$$h^2\Omega_{\rm GW,\ SMBHB}(f) = \frac{2\pi^2}{3H_0^2}A^2\left(\frac{f}{\rm year^{-1}}\right)^{5-\gamma}{\rm year}^2, \tag{4.2}$$

with h the dimensionless Hubble parameter, H_0 the Hubble rate evaluated today and A and γ two free parameters. Analysing PTA data for such a model thus consists in defining prior distributions for the parameters A and γ, assuming a likelihood that depends, with other ingredients, on the SMBHB power-law model given in Eq. (4.2) and computing the posterior probability distributions of the parameters A and γ. Another traditional data analysis for PTA data is to assume a free-spectrum i.e. to assume no constraint on the GW spectrum allowing a complete flexibility in the modelling in each frequency bin. The resulting data analysis consists in the NANOGrav free-spectrum posteriors in each frequency bin usually referred to as the 30 violins because of their shape.

The code used in this project to analyse PTA data is PTArcade [31, 32]. PTArcade is a publicly available code. PTArcade provides a way to perform Bayesian analysis of new-physics GW spectra with PTA data. Using PTArcade consists in providing a GW spectrum $\Omega_{\rm GW}(f, \vec{\theta})$ with f the frequency today and $\vec{\theta}$ an array containing the free parameters of the GW spectrum and prior distributions for all the parameters contained in $\vec{\theta}$. As the evidence ($p(d)$ in Eq. (4.1)) can not be computed in a closed-form way, PTArcade performs a Markov chain Monte Carlo (MCMC) to approximate the resulting posteriors. PTArcade computes the Markov chain using Metropolis-Hastings algoritm. This algorithm consists in first choosing a random point in the parameter space. PTArcade computes the cross-correlation of the timing residuals between pairs of pulsars for the given parameters and compare the result with PTA data. Then, a second point in the parameter space is chosen randomly and the cross-correlation of the timing residuals between pairs of pulsars for this second set of parameters is again compared to PTA data. After comparing two sets of parameters, the following probability P, called the acceptance, is computed:

$$P = \frac{\frac{p(d|\theta_2)p(\theta_2)}{p(d)}}{\frac{p(d|\theta_1)p(\theta_1)}{p(d)}} = \frac{p(d|\theta_2)p(\theta_2)}{p(d|\theta_1)p(\theta_1)}, \tag{4.3}$$

where θ_1 is the first set of parameters and θ_2 the second set of parameters. If the resulting probability satisfies $P \geq 1$, the second point in parameter space is accepted. If the resulting probability satisfies $P \leq 1$, the second point in the parameter space is rejected with probability $1 - P$ and accepted with probability P. If the second set of parameters is accepted, it means that the set is kept in the MCMC chain and then, the algorithm jumps to another point of the parameter space in the vicinity of this second point and performs the analysis again. If the second set of parameters is rejected, it means that the set is not kept in the MCMC chain and then, the algorithm jumps to a random point of the parameter space in the vicinity of the first point and performs the analysis again. The output of PTArcade is then a list of the accepted points in parameter space. It is important to note here that PTArcade fits the GW model to the first 14 frequency bins (corresponding to the the first 14 violins) of the PTA data because it is assumed that the data in the next bins is dominated by white noise.

The input of PTArcade consists in two files: the model file and the configuration file. In the model file, the free parameters are defined with their prior distributions and the GW spectrum $\Omega_{\rm GW}$ is defined as a function of frequency today f. The model file also contains the parameter "smbhb". If set to "True", the GW model analyzed by PTArcade is the GW model defined in the model file together with the SMBHB power-law model given in Eq. (4.2). The priors for the parameters A and γ from the SMBHB power-law model are parameterized in PTArcade as 2D Gaussian priors which were fitted to the distribution of the parameter A and γ derived by performing a power-law fit to the SMBHB populations simulated in [29] (see Fig.6 in Appendix B). The configuration file contains additional options. It contains the parameter "pta_data" that specifies the PTA data set used in the analysis. For this project, the parameter "pta_data" is set to "NG15" that corresponds to the set of PTA data collected by the NANOGrav collaboration over 15 years. The configuration file also contains the parameter "N_samples" that is the number of points that will be generated by the Monte Carlo sampler and which is set to 2^6 in this project. The last important parameter defined in the configuration file is the parameter "model_sel" that can be set to "False" or "True". If set to "True", this option allows to compare the GW spectrum defined in the model file to the SMBHB power-law model. This option allows to evaluate how the model given in the model file improves the PTA data fit or not compared to the PTA data fit of the SMBHB power-law model. Along with this option, PTArcade computes the Bayes factor B defined as $B = p(d|M1)/p(d|M2)$ for $M_{1,2}$ two different models such that $B > 1$ means that $M1$ is more strongly supported by the data than $M2$ or in other word, that $M1$ gives a better fit to the data than $M2$. In the case of PTArcade, the model of reference is the SMBHB power-law model such that $B > 1$ means that the model defined in the model file is more supported by the data than the SMBHB power-law model [8].

[8] The Bayes factor is calculated by dividing the number of points in the chain that fall in the hypermodel bin of the user-specified signal by the number of points falling in the bin of the reference SMBHB power-law model, see [31, 32] for more details.

Finally, PTArcade is launched via a ".sh" file containing information about the number of MC chains that run simultaneously, that is set to 10 in this project and about the number of days PTArcade runs, that is set to 14 in this project [9].

4.2 Production of gravitational waves: numerical setup

The aim of this section is to express the analytical results from the previous sections in a form that corresponds to the input of PTArcade, in order to perform a Bayesian analysis of the inflationary axion-$U(1)$ spectator model with the PTA data collected by the NANOGrav collaboration. The first step is thus to determine the free parameters of the model for fixed values of the parameter δ. The second step is to derive the corresponding GW spectrum as a function of frequency today and of the free parameters.

The free parameters of the inflationary axion-$U(1)$ spectator model The fine structure constant α of the $U(1)$ sector that the axion σ couples to is let unspecified and is therefore a free parameter. The same is true for the decay constant f of the axion σ, the constant Λ that characterizes the height of the axion potential V_σ and the Hubble rate H. Finally, the time t_* at which the axion velocity is maximal depends on the initial value of the axion σ that is let unspecified. The time t_* (and correspondingly the conformal time τ_*) is thus also a free parameter.
From Eq. (3.28), the Hubble rate H is directly related to the vacuum tensor-to-scalar ratio $r_{\rm vac}$ that becomes the new free parameter. Performing a rescaling of the axion $\sigma \to \sigma/f \equiv \theta$ does not change the dynamics. With this rescaling, the axion potential becomes $V_\sigma(\sigma) \to V_\theta(\theta) = (\Lambda^4/f^2)[\cos\theta + 1]$ and the parameters Λ and f always appear via the combination Λ^4/f^2. Considering this combination as a new free parameter allows to reduce the number of free parameters by one. In addition, the fixed parameter δ is defined as $\delta \equiv (\Lambda^4/f^2)/(6H^2) \Rightarrow \Lambda^4/f^2 = 6\delta H^2$. The combination Λ^4/f^2 is thus the same free parameter as the Hubble rate H for fixed values of the parameter δ and therefore depends on the free parameter $r_{\rm vac}$.
It is important to note here that the trick of introducing the rescaling $\sigma \to \sigma/f \equiv \theta$ that allows to reduce the number of free parameters holds only in the low-backreaction regime. Indeed, in the strong backreaction regime, the coupling term between the axion and the gauge field affects the dynamics of the axion σ and the free parameter f appears independently of the combination Λ^4/f^2. In that case, it would be necessary to treat the parameters Λ and f as two independent free parameters.
The parameter ξ_* is given by $\xi_* = \alpha\delta/2$. As the parameter α is free, the parameter ξ_* can be chosen as the free parameter for fixed values of the parameter δ.
The critical comoving wavenumber k_* is defined as $k_* \equiv \tau_*^{-1}$ and is therefore a free parameter. The comoving wavenumber k is related to the frequency today f via the relation:

$$f = \frac{1}{2\pi}\frac{k}{a_0}, \tag{4.4}$$

where a_0 is the scale factor evaluated today. Therefore, a critical frequency f_* can be introduced that is related to the critical comoving wavenumber k_* via Eq. (4.4). This critical frequency f_* is chosen as the free parameter.
To sum up, for fixed values of the parameter δ, three free parameters arise from the model: the critical frequency f_*, the parameter ξ_* and the vacuum tensor-to-scalar ratio $r_{\rm vac}$. These three parameters will be the free parameters of the statistical analysis.

The GW spectrum produced by the inflationary axion-$U(1)$ spectator model An inflationary GW spectrum $\Omega_{\rm GW}$ in the PTA frequencies given as a function of frequency today is related to the tensor power spectrum $\mathcal{P}$ by [29]:

$$\Omega_{\rm GW}(f) = \frac{\Omega_r}{24}\frac{g_*(f)}{g_*^0}\left(\frac{g_{*,s}^0}{g_{*,s}(f)}\right)^{4/3}\mathcal{P}(f)\mathcal{T}(f), \tag{4.5}$$

where Ω_r/g_*^0 is the current radiation energy density per relativistic degree of freedom, in units of the critical (closure) density, $g_{*,s}^0$ counts the effective number of relativistic degrees of freedom contributing to the radiation entropy today, $g_*(f)$ and $g_{*,s}(f)$ denote the effective numbers of relativistic degrees of freedom in the early universe when GWs with comoving wavenumber k re-enter the Hubble horizon during the reheating stage after inflation and $\mathcal{T}(f)$ is the transfer function that accounts for the redshifting behavior of GWs that re-enter the horizon during the reheating stage after inflation. For a sufficiently large reheating temperature, the transfer function only affects GWs at frequencies above the PTA frequency band, meaning that the transfer function can be neglected for the purposes of this work. The current radiation energy density per relativistic degree of freedom Ω_r/g_*^0 and the effective number of relativistic degrees of freedom contributing to the radiation entropy today $g_{*,s}^0$ are measured quantities given by [29]:

$$\frac{\Omega_r}{g_*^0} \approx 2.72\cdot 10^{-5} \quad g_{*,s}^0 \approx 3.93. \tag{4.6}$$

[9] The run of this project, that comes with different configurations, has been launched on the cluster of the university of Münster.

Putting everything together, the GW spectrum $\Omega_{\rm GW}$ of the inflationary axion-$U(1)$ spectator model in the PTA frequencies as a function of frequency today and of the free parameters f_*, ξ_* and $r_{\rm vac}$ is given by [10]:

$$\Omega_{\rm GW}(f) = \frac{1}{24}(5.71\cdot 10^{-14})\left(\frac{3.93}{g_{*,s}(f)}\right)^{4/3} g_*(f)\frac{r_{\rm vac}}{2}\left[1+\frac{r_{\rm vac}}{128}(2.1\cdot 10^{-9})p\left(\frac{f}{f_*},\xi_*,\delta\right)\right],$$

$$p\left(\frac{f}{f_*},\xi_*,\delta\right) = \begin{cases} e^{(-7.98+10\xi_*+0.0979\xi_*^2)}\exp\left[-\dfrac{1}{2(1.38-0.178\xi_*+0.0103\xi_*^2)}\ln^2\left(\dfrac{f}{f_*(5.45+0.455\xi_*+0.0316\xi_*^2)}\right)\right] & ,\ \delta=0.2 \\ e^{(-6.85+9.05\xi_*+0.0596\xi_*^2)}\exp\left[-\dfrac{1}{2(0.768-0.993\xi_*+0.00608\xi_*^2)}\ln^2\left(\dfrac{f}{f_*(2.7+0.896\xi_*+0.0187\xi_*^2)}\right)\right] & ,\ \delta=0.5. \end{cases} \tag{4.7}$$

The GW spectrum given in Eq. (4.7) will be the GW spectrum defined in the model file of PTArcade.

4.3 Numerical results from PTArcade

Two different runs have been launched. The first run is the analysis of the inflationary axion-$U(1)$ spectator model. This run is denoted (M1). The second run is the analysis of the inflationary axion-$U(1)$ spectator model to which the SMBHB power-law model given in Eq. (4.2) is added. This run is denoted (M2). Two additional runs have been launched, that correspond to the runs (M1) and (M2) with the parameter "model_sel" set to "True". These runs allow to compute the Bayes factors.

The results of PTArcade Bayesian analysis are presented Fig.4. The prior distributions of the free parameters f_*, $r_{\rm vac}$ and ξ_* are chosen as uniform distributions as:

$$U_{\log_{10}(f_*)} = U(-10,-6) \quad U_{\log_{10}(r_{\rm vac})} = U(-5,0) \quad U_{\xi_*} = U(4,8), \tag{4.8}$$

where $U(a,b)$ denotes the uniform distribution with bounds $[a,b]$ and U_X denotes the uniform distribution of the parameter X.
The runs (M1) and (M2) with parameter "model_sel" set to "True" give the following Bayes factors B [11]:

$$B = \begin{cases} 4.91\pm 0.35,\ \delta=0.2 \quad \text{(M1)} \\ 8.03\pm 0.35,\ \delta=0.2 \quad \text{(M2)} \\ 0.0104\pm 0.0029,\ \delta=0.5 \quad \text{(M1)} \\ 1.19\pm 0.03,\ \delta=0.5 \quad \text{(M2)}. \end{cases} \tag{4.9}$$

Fig.5 presents the GW spectra of the runs (M1) and (M2) computed with free parameters evaluated at the mean values of the MCMC chains, allowing a qualitative discussion of the results. The NANOGrav free spectrum is also displayed as comparison [12].

NB: *For now on, the following shortcut notation will be used. The GW spectrum produced by the inflationary axion-$U(1)$ spectator model will be referred to as the "Axion spectator" spectrum or the "Axion spectator" contribution in the case of the run (M2). The GW spectrum corresponding to the SMBHB power-law model given in Eq. (4.2) will be referred to as the "SMBHB" spectrum or the "SMBHB" contribution in the case of the run (M2). The model (M2) will be denoted as the "Axion spectator + SMBHB" model. Quantities computed setting $\delta = 0.2$ will be labelled (S) for "small δ" and quantities computed setting $\delta = 0.5$ will be labelled (L) for "large δ".*

Results from the run (M1) From Fig.4a and Fig.4b, in both cases of "small δ" and "large δ", the results from the run (M1) give marginally trustworthy results as the 68% and 95% Bayesian credible regions in the 2D posterior distribution $(\log_{10}(r_{\rm vac}),\xi_*)$ are within the low-backreaction regime (that lies above the dashed black line) but close to the upper bound. These results can therefore be analyzed more in details. For the run (M1), the 1D marginalized distribution of $\log_{10}(f_*)$ for the parameter f_* presents a sharp peak: $\log_{10}(f_*^{(S)}) \sim -8.75$ and $\log_{10}(f_*^{(L)}) \sim -9.1$. This indicates a strong constraint on the parameter f_*, one value being well preferred. This constraint on the parameter f_* impacts the results of the parameters $r_{\rm vac}$ and ξ_* by putting strong constraints as indicated in the 2D posterior distributions $(\log_{10}(f_*),\log_{10}(r_{\rm vac}))$ and $(\log_{10}(f_*),\xi_*)$. The 68% and 95% Bayesian credible regions are indeed well defined and centered around the preferred value of the parameter f_*. In particular, from the 2D posterior distribution $(\log_{10}(f_*),\xi_*)$, the 68% Bayesian credible region gives the bounds: $4.6 < \xi_*^{(S)} < 6.6$ and $4.9 < \xi_*^{(L)} < 7.1$. The 1D marginalized distribution of the parameter ξ_* indicates that there is actually a preferred value for the parameter ξ_*: $\xi_*^{(S)} \sim 4.5$ and $\xi_*^{(L)} \sim 5$. Concerning the parameter $r_{\rm vac}$, the 68% and 95% Bayesian credible regions of the 2D posterior distribution $(\log_{10}(f_*),\log_{10}(r_{\rm vac}))$ do not give lower and upper bounds on the parameter $r_{\rm vac}$. However, the 2D posterior distribution $(\log_{10}(r_{\rm vac}),\xi_*)$ indicates that increasing the value of the parameter ξ_* implies decreasing the parameter $r_{\rm vac}$, giving a strong combined constraint on these parameters.

[10] The functions $g_*(f)$ and $g_{*,s}(f)$ are let unspecified here because they are defined in a specific package of PTArcade.
[11] The uncertainties on the Bayes factors are computed using a statistical bootstrapping [33].
[12] The NANOGrav free spectrum is a set of publicly available data that the Münster team gave me in order to plot the figure given in Fig.5.

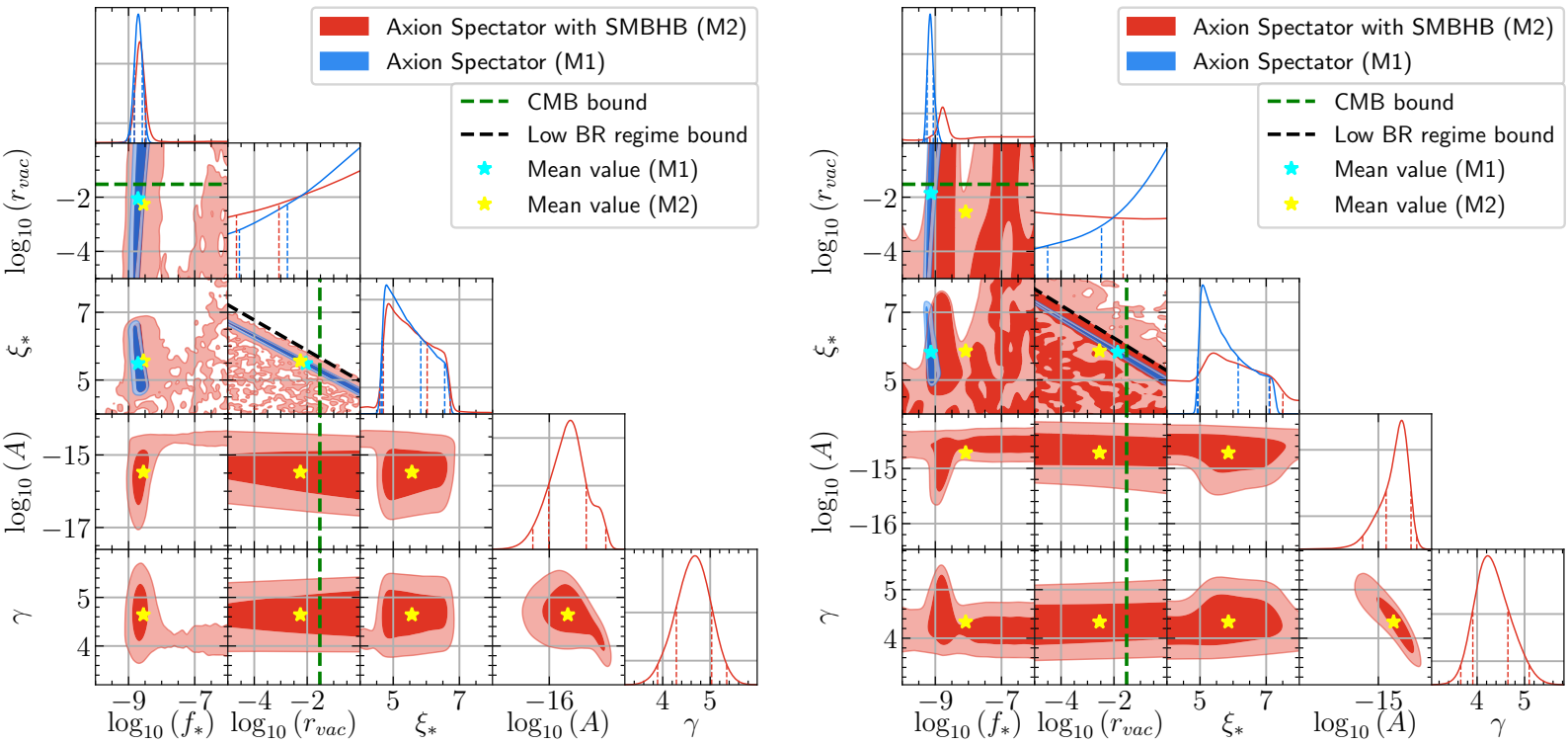

(a) (b)

Figure 4: Reconstructed posterior distributions for the parameters f_*, $r_{\rm vac}$ and ξ_* of the inflationary axion-$U(1)$ spectator model given in Eq. (4.7) and the parameters A and γ of the SMBHB power-law model given in Eq. (4.2). The label (M1) denotes the analysis of the inflationary axion-$U(1)$ spectator model alone and the label (M2) denotes the analysis of the inflationary axion-$U(1)$ spectator model with the SMBHB power-law model. On the diagonal of the corner plot, the 1D marginalized distributions together with the 68% and 95% Bayesian credible intervals (vertical lines) are reported, while on the off-diagonal panels, the 68% (darker) and 95% (lighter) Bayesian credible regions in the 2D posterior distributions are reported. All credible intervals and regions are constructed by integrating over the regions of highest posterior density. The CMB bound corresponds to the measured constraint $r_{\rm vac} < 0.03$ [30] and the low-backreaction, labelled "low BR", regime bound corresponds to the constraints given in Eq. (3.29). The mean values of the MCMC chains are also displayed as star symbols. (a) $\delta = 0.2$ (b) $\delta = 0.5$.

A simple linear fit gives the relations: $\xi_*^{(S)} = -0.4\log_{10}(r_{\rm vac}^{(S)}) + 4.6$ and $\xi_*^{(L)} = -0.44\log_{10}(r_{\rm vac}^{(L)}) + 4.9$. For the associated GW spectrum presented Fig.5 as a dashed blue curve, varying the parameter f_* moves the resulting spectrum to the right or to the left, whereas varying the parameter $r_{\rm vac}$ varies the amplitude of the spectrum and varying the parameter ξ_* moves the spectrum in both directions. The precise preferred value of the parameter f_* thus indicates a precisely centered GW spectrum in frequencies. A decrease in the parameter $r_{\rm vac}$ reduces the strength of the spectrum, but this can be compensated by an increase in the parameter ξ_*. This means that while moving along the lines $\xi_*^{(S)} = -0.4\log_{10}(r_{\rm vac}^{(S)}) + 4.6$ and $\xi_*^{(L)} = -0.44\log_{10}(r_{\rm vac}^{(L)}) + 4.9$ both effects balance out: smaller parameter $r_{\rm vac}$ makes the spectrum weaker, larger parameter ξ_* makes the spectrum stronger, such that, along this straight lines, the strength of the spectrum remains the same. In conclusion, the combination of the parameters $r_{\rm vac}$ and ξ_* adjusts the GW spectrum on top of the NANOGrav free spectrum. The mean values of the MCMC chains for each parameter are given by: $< \log_{10}(f_*^{(S)} >= -8.71$, $< \log_{10}(r_{\rm vac}^{(S)}) >= -2.05$, $< \xi_*^{(S)} >= 5.49$, $< \log_{10}(f_*^{(L)}) >= -9.13$, $< \log_{10}(r_{\rm vac}^{(L)}) >= -1.86$ and $< \xi_*^{(L)} >= 5.81$. These values are a good choice as reference values as they are consistent with the peak values appearing in the 1D marginalized distributions of the parameters f_* and ξ_*, lie in the 68% Bayesian credible regions of all 2D posterior distributions and are within the low-beackreaction regime as well as within the acceptance regime from the CMB constraint. These values are therefore the ones chosen to construct the illustrative plot of the GW spectrum presented Fig.5. From Fig.5a, it appears that in the case of "small δ", the "Axion spectator" spectrum computed with the parameters evaluated at the mean values of the MCMC chains agrees with the NANOGrav free spectrum in the first 14 frequency bins. From Fig.5b that corresponds to the case of "large δ", it appears also that the "Axion spectator" spectrum computed with the parameters evaluated at the mean values of the MCMC chains agrees with the NANOGrav free spectrum in the first frequency bins but in a shorter range of frequencies than the case of "small δ". Finally, the values of the Bayes factor for the run (M1) given in Eq. (4.9) allow to conclude that for the case of a "small δ", the "Axion spectator" model gives a better fit to PTA data than the "SMBHB" model as $B^{(S)} > 1$. For the case of a "large δ", the Bayes factor given in Eq. (4.9) satisfying $B^{(L)} < 1$, the "Axion spectator" model does not give a better fit to PTA data than the "SMBHB" model.

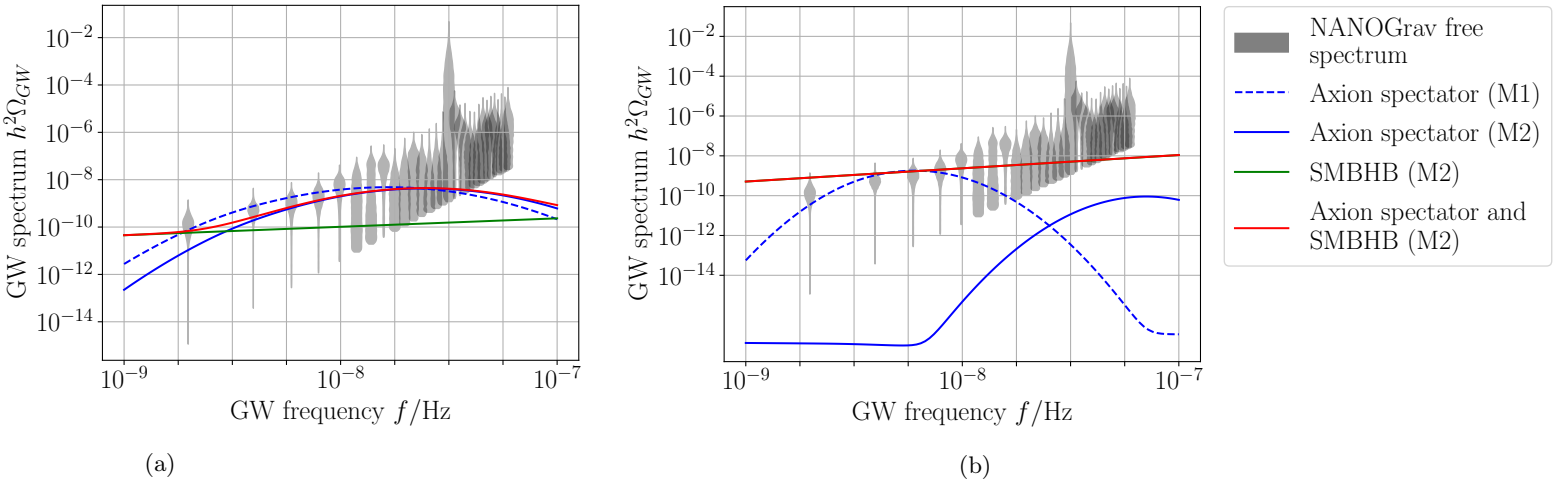

Figure 5: GW spectrum of the model given in Eq. (4.7). The label (M1) denotes the analysis of the model given in Eq. (2.1) alone and the label (M2) denotes the analysis of the model given in Eq. (2.1) with the power-law model of SMBHB given in Eq. (4.2). The values of the parameters are chosen as being the mean values presented in Fig.4. The NANOGrav free spectrum is also displayed in grey (a) $\delta = 0.2$ (b) $\delta = 0.5$.

Results from the run (M2) From Fig.4a corresponding to the case of "small δ", the results from the run (M2) give marginally trustworthy results as the 68% and 95% Bayesian credible regions in the 2D posterior distribution $(\log_{10}(r_{\rm vac}), \xi_*)$ are within the low-backreaction regime but close to the upper bound. In the same way, from Fig.4b corresponding to the case of "large δ", the run (M2) gives marginally trustworthy results as the 68% Bayesian credible regions in the 2D posterior distribution $(\log_{10}(r_{\rm vac}), \xi_*)$ lie within the low-backreaction regime. However, some 95% Bayesian credible regions in the 2D posterior distribution $(\log_{10}(r_{\rm vac}), \xi_*)$ are outside the low-backreaction regime and therefore these regions must be excluded as lying in the regime of non-validity of this work. These regions excluded, the results can be analyzed in more details. In the case of "small δ", the 68% Bayesian credible regions in the 2D posterior distributions for the parameters f_*, $r_{\rm vac}$ and ξ_* overlap almost exactly the 68% Bayesian credible regions form run (M1). Therefore, in the case of "small δ", the results form the run (M2) for the parameters f_*, $r_{\rm vac}$ and ξ_* are the same as for the run (M1). For both cases of "small δ" and "large δ", the 1D marginalized distributions of $\log_{10}(f_*)$ for the parameter f_* present a peak less sharp than in the run (M1). This induces allowed values of the parameter f_* in higher frequencies. In the case of "small δ", this translates into 95% Bayesian credible regions in the 2D posterior distributions for all parameters at higher frequencies. In the case of "large δ", the peak in the 1D marginalized distribution of $\log_{10}(f_*)$ being even less sharp more values are allowed at high frequencies. As a consequence, 68% Bayesian credible regions in the 2D posterior distributions for all parameters appear at high frequencies. These regions correspond to frequencies around 10^{-7}Hz that do not lie in PTA frequencies range. Therefore, there exists no data for such frequencies. These results can be explained as follows. As there are no data in high frequencies, the parameters can take almost any values because there exists no GW spectrum of reference in that range of frequencies. As a consequence, the mean values of all parameters are displaced to higher frequencies compared to the run (M1). These mean values are given by: $< \log_{10}(f_*^{(S)}) >= -8.55$, $< \log_{10}(r_{\rm vac}^{(S)}) >= -2.26$, $< \xi_*^{(S)} >= 5.56$, $< \log_{10}(f_*^{(L)}) >= -8.08$, $< \log_{10}(r_{\rm vac}^{(L)}) >= -2.55$ and $< \xi_*^{(L)} >= 5.86$. Concerning the parameters A and γ of the "SMBHB" contribution, in the case of "small δ", the 68% Bayesian credible region gives the bounds:$-16.1 < \log_{10}(A^{(S)}) < -15$ and $3.8 < \gamma^{(S)} < 4.8$ and the mean values of the MCMC chains are given by $< \log_{10}(A^{(S)}) >= -15.5$ and $< \gamma^{(S)} >= 4.6$. By comparing the posterior distribution with the prior distribution (see regions delimited by the dashed black curves in Fig.6 in Appendix B) in the case of "small δ", it appears that the 68% Bayesian credible region of the 2D posterior distribution $(\log_{10}(A), \gamma)$ is slightly displaced compared to the prior distribution but very similar. This already suggests that as the run (M1) gives a good fit to PTA data, adding the "Axion spectator" model to the "SMBHB" model improves the PTA data fit and therefore the parameters A and γ of the "SMBHB" contribution are not constrained. The value of the Bayes factor given in Eq. (4.9) being greater than unity, it means that the model "Axion spectator + SMBHB" is more strongly supported by the data than the model "SMBHB" alone. In the case of "large δ", the 68% Bayesian credible region of the 2D posterior distribution $(\log_{10}(A), \gamma)$ gives the constraints $-15 < \log_{10}(A^{(L)}) < -14$ and $3.7 < \gamma^{(L)} < 4.8$ leading to mean values $< \log_{10}(A^{(L)}) >= -14.7$ and $< \gamma^{(L)} >= 4.33$. By comparing the posterior distribution with the prior distribution, it appears that a large region of the prior distribution is excluded by the posterior distribution. This already suggests that, as the run (M1) does not give a good fit to the PTA data (see the Bayes factor given in Eq. (4.9)) in the case of "large δ", adding the "Axion spectator" contribution to the "SMBHB" contribution does not improve much the PTA data fit and therefore the parameters A and γ of the "SMBHB" contribution are strongly constrained. This is confirmed by the value of the Bayes factor given in Eq. (4.9). In the case of "large δ", the value of the Bayes factor given in Eq. (4.9) is slightly greater than unity meaning that the model "Axion spectator + SMBHB" is slightly more strongly supported by the data than the model "SMBHB" alone. As for the run (M1), the mean values of the MCMC chains are a good choice of reference values as they lie in the 68% Bayesian credible regions of

all 2D posterior distributions and are within the low-beackreaction regime as well as within the acceptance regime from the CMB constraint. The GW spectra presented Fig.5 for the run (M2) are therefore computed with values of the parameters evaluated at the mean values of the MCMC chains. The solid blue and green curves that are presented on Fig.5 correspond to the two separated contributions, respectively the "Axion spectator" contribution and the "SMBHB" contribution computed in the run (M2). The total GW spectrum is given by the solid red curve. From Fig.5a, it appears that adding the "Axion spectator" contribution induces a bump in the total GW spectrum compared the "SMBHB" contribution. This allows to confirm qualitatively that in the case of "small δ", adding the "Axion spectator" contribution to the "SMBHB" contribution improves the fit of the PTA data. From Fig.5b, the total GW spectrum "Axion spectator + SMBHB" is completely dominated by the "SMBHB" contribution as the green and red curves overlap. This confirms the fact that adding the "Axion spectator" contribution does not improve much the "SMBHB" fit of the PTA data in the case of "large δ".

By comparing all the Bayes factors given in Eq. (4.9), it appears that the model "Axion spectator + SMBHB" for a "small δ" is the model that improves the "SMBHB" model alone the most.

4.4 Constraints on the inflationary axion-$U(1)$ spectator model

In the previous section, the results from the Bayesian statistical analysis from PTArcade with the inflationary axion-$U(1)$ spectator model and with the SMBHB power-law model have been presented. The aim of this section is to discuss the results presented in the previous sections. Constraints of the free parameters of the inflationary axion-$U(1)$ spectator model such as the number of e-folds ΔN that separates the moment when the CMB scale leaves the horizon and the moment when the axion velocity is maximal, the fine structure constant α, the Hubble rate H and the height of the axion potential Λ^4 are derived.

The inflationary axion-$U(1)$ spectator model as a source of PTA data Let's focus on the run (M1).
As the peak in the 1D marginalized distribution of the parameter f_* is very sharp, constraining the parameter f_* to its mean value is a good approximation. The parameter f_* is related to the parameter k_*, the comoving wavenumber, via Eq. (4.4) and corresponds to the scale that leaves the horizon at time $t = t_*$ when the axion velocity is maximal. In addition, as the comoving wavenumber k is related to the scale factor via the relation at physical time t $k = a(t)H$, this leads to: $k_* = a(t_*)H = e^{N_*}H$ where N_* is the number of e-folds at physical time $t = t_*$. It is possible to relate the comoving wavenumber k_* to the comoving wavenumber $k_{\rm CMB} = a(t_{\rm CMB})H = e^{N_{\rm CMB}}H$ that corresponds to the CMB scale that leaves the horizon at physical time $t = t_{\rm CMB}$ or correspondingly at $N_{\rm CMB}$ e-folds. The comoving wavenumber $k_{\rm CMB}$ is usually evaluated as $k_{\rm CMB} = 5 \cdot 10^{-16}$Hz [26]. Therefore, it is possible to evaluate the number of e-folds ΔN that separates the time at which the CMB scale leaves the horizon and the time at which the scale corresponding to k_* leaves the horizon. This reads: $k_*/k_{\rm CMB} = e^{\Delta N}$ or in frequency $f_*/f_{\rm CMB} = e^{\Delta N}$. Using the mean values of the MCMC chains for the parameter f_*: $\Delta N^{(S)} = 17$ and $\Delta N^{(L)} = 16$ setting the value of the scale factor today to unity. This means that in order for the GW spectrum produced by the inflationary axion-$U(1)$ spectator model to fit PTA data, if the case is of "small δ", then 17 e-folds should separate the moment when the CMB scale leaves the horizon and the moment when the axion velocity is maximal. In the case of "large δ", 16 e-folds should separate the moment when the CMB scale leaves the horizon and the moment when the axion velocity is maximal.
The parameter ξ_* is directly related to the fine structure constant α of the $U(1)$ sector the axion couples to and therefore the 68% Bayesian credible constraint on the parameter α reads: $46 < \alpha^{(S)} < 66$ and $19.6 < \alpha^{(L)} < 28.4$. This means that in order for the GW spectrum produced by the inflationary axion-$U(1)$ spectator model to fit PTA data, if the case is of "small δ", the fine structure constant α of the $U(1)$ sector the axion couples to should verify $46 < \alpha < 66$. In the case of "large δ", the fine structure constant α of the $U(1)$ sector should verify $19.6 < \alpha < 28.4$. These values of the fine structure constant are rather large if compared for instance to the fine structure constant in quantum electrodynamics that is approximately 1/137. Such large values present a challenge for model building. It indeed rises the theoretical question of whether it is actually possible to construct UV completions of the inflationary axion-$U(1)$ spectator model that really allows for such large values of the fine structure constant of the $U(1)$ sector.
As already pointed out, in order for the GW spectrum produced by the inflationary axion-$U(1)$ spectator model to fit PTA data, the vacuum tensor-to-scalar ratio $r_{\rm vac}$ and the parameter ξ_* should satisfy $\xi_*^{(S)} = -0.4 \log_{10}(r_{\rm vac}^{(S)}) + 4.6$ with $4.6 < \xi_*^{(S)} < 6.6$, $\xi_*^{(L)} = -0.44 \log_{10}(r_{\rm vac}^{(L)}) + 4.9$ with $4.9 < \xi_*^{(L)} < 7.1$ as well as $r_{\rm vac}^{(S,L)} < 0.03$ given by the CMB measurements. Putting everything together leads to the constraint on the parameter $r_{\rm vac}$: $10^{-5} < r_{\rm vac}^{(S,L)} < 0.03$ where the lower bound is the lower bound of the prior range and is therefore imposed by hand. This means that no constraint on the parameter $r_{\rm vac}$ arises from the PTArcade data analysis. From Eq. (3.28), this constraint on the parameter $r_{\rm vac}$ can be translated into a constraint on the Hubble rate that reads: $7.73 \cdot 10^{11}$GeV $< H < 4.23 \cdot 10^{13}$GeV (note that the labels (S, L) are dropped here because the result is the same in both cases of "small δ" and "large δ"). The linear relations that arise from the PTArcade Bayesian analysis between the parameters ξ_* and $r_{\rm vac}$ translate into the constraints on the Hubble rate H and the fine structure constant α of the $U(1)$ sector as: $\alpha^{(S)} = -4 \log_{10}(1.68 \cdot 10^{-29} H^2) + 46$ and $\alpha^{(L)} = -1.76 \log_{10}(1.68 \cdot 10^{-29} H^2) + 19.6$. Finally, the considerations given in Sec.4.2 allow to derive the following constraints on the combination Λ^4/f^2: $7.16 \cdot 10^{23} < (\Lambda^4/f^2)^{(S)} < 7.18 \cdot 10^{28}$ and $1.80 \cdot 10^{24} < (\Lambda^4/f^2)^{(L)} < 1.79 \cdot 10^{29}$. From the definition of the decay constant f of the axion σ, f corresponds to the scale at which the spontaneous symmetry

breaking (SSB) of the axion potential occurs. In order for an axion to be spectator during inflation, this SSB should occur before inflation and therefore the decay constant f of the axion σ should be greater than the inflation scale. To ensure that the decay constant f is greater than the inflation scale, it is possible to impose $f \sim M_P \sim 10^{18}$GeV. Consequently, the constraint on the combination Λ^4/f^2 becomes a constraint on the height of the axion potential Λ^4 alone that reads: $9.20 \cdot 10^{14}\text{GeV} < \Lambda^{(S)} < 1.16 \cdot 10^{16}\text{GeV}$ and $1.16 \cdot 10^{15}\text{GeV} < \Lambda^{(L)} < 2.06 \cdot 10^{16}\text{GeV}$. This means that in order for the GW spectrum produced by the inflationary axion-$U(1)$ spectator model to fit PTA data, if the case is of "small δ", the height of the axion potential Λ^4 should verify $9.20 \cdot 10^{14}\text{GeV} < \Lambda < 1.16 \cdot 10^{16}\text{GeV}$. In the case of "large δ", the height of the axion potential Λ^4 should verify $1.16 \cdot 10^{15}\text{GeV} < \Lambda < 2.06 \cdot 10^{16}\text{GeV}$.

The inflationary axion-$U(1)$ spectator model with the SMBHB power-law model as a source of PTA data
Let's focus on the run (M2).
As already pointed out in Sec.4.3, in the case of "small δ", from the results of the posterior distributions given in Fig.4a, the 68% Bayesian credible regions in the 2D posterior distributions from the run (M2) for the parameters f_*, r_{vac} and ξ_* overlap almost exactly the 68% Bayesian credible regions form run (M1). Therefore, in the case of "small δ", in order for the inflationary axion-$U(1)$ spectator with SMBHB power-law model to fit PTA data, the number of e-folds ΔN that separates the moment when the CMB scale leaves the horizon and the moment when the axion velocity is maximal, the fine structure constant α, the Hubble rate H and the height of the axion potential Λ^4 of the inflationary axion-$U(1)$ spectator model contribution are subjects to the same constraints as in the previous paragraph. Concerning the parameters A and γ of the SMBHB power-law contribution, these parameters are not constrained compared to their prior distributions.
In the case of "large δ", it has been pointed out Sec.4.3 that the peak in the parameter f_* not being sharp induces allowed values of the parameters ξ_* and r_{vac} at high frequencies. Consequently, no constraints can be derived on the parameters f_*, ξ_* and r_{vac} and therefore, the parameters ΔN, α, H and Λ^4 are not constrained. In contrast, the parameters A and γ of the SMBHB power-law model are strongly constrained and the region $\gamma^{(L)} > 5, \log_{10}(A^{(L)}) < -15$ is excluded from the prior distribution. Therefore, in the case of "large δ", in order for the inflationary axion-$U(1)$ spectator with SMBHB power-law model to fit PTA data, the number of e-folds ΔN that separates the moment when the CMB scale leaves the horizon and the moment when the axion velocity is maximal, the fine structure constant α, the Hubble rate and the height of the axion potential Λ^4 are not constrained. The parameters A and γ of the SMBHB power-law contribution are strongly constrained and the region $\gamma > 5, \log_{10}(A) < -15$ should be excluded.

5 Conclusion

Phenomenological considerations such as the need of the degrees of freedom from inflation to decay when inflation ends motivates to study an inflationary model where inflation is driven by an inflaton field and add a spectator axion field coupled to a $U(1)$ gauge field: the inflationary axion-$U(1)$ spectator model studied in this work.
In the low-backreaction regime, studying the dynamics of the slowly rolling axion field allows to introduce an important parameter denoted δ that is approximately a measure of the relative change of the axion field value during one Hubble time at the top of its potential. This parameter δ being commonly taken equal to $\delta = 0.2, 0.5$ in literature, this is also the choice made in this work.
In the low-backreaction regime, if the axion field is slowly rolling and therefore its velocity is non-zero, a tachyonic mass term appears in the equation of motion of the plus polarization of the gauge field at large scales. Solving this equation of motion requires to perform a semi-analytical computation, namely the Wentzel Kramers Brouillouin approximation. This computation allows to derive an approximate solution for the plus polarization of gauge field that is valid at large scales. This solution is exponentially growing, meaning that an exponential production of quanta of the gauge field of plus polarization occurs. Introducing tensor perturbations of the metric, it appears that the gradients of the gauge field source tensor perturbations of the metric. As the plus polarization of the gauge field is amplified exponentially, its gradients are non-zero and therefore source tensor perturbations. In sum, the coupling between the axion field and the gauge field sources tensor perturbations because the axion field is slowly rolling. These tensor perturbations undergo the phenomenon due to the exponential expansion of universe: they are stretch to cosmological scales, become classical, leave the horizon and freeze out. They re-enter the observable universe during the reheating stage after inflation leading to GWs. In particular, it appears that GWs with plus polarization are more produced than GWs with minus polarization. This means that one signature of GWs produced during inflation via a coupling between an axion field and a $U(1)$ gauge field is their chirality: the GWs have the same polarization as the amplified gauge field mode.
The related GW spectrum produced by the inflationary axion-$U(1)$ spectator model can thus be computed analytically via the tensor power spectrum whose expression is highly model-dependent. But this GW spectrum can also be detected. One way of detecting GWs is to use pulsars via measuring the correlated pulse time arrival delays between several pulsars. The NANOGrav collaboration used this technique called PTA to recently release a 15 year PTA data set yielding a strong evidence of a GW spectrum. The motivation of this project is the work of Caner Unal, Alexandros Papageorgiou and Ippei Obata [17]. In this work, the GW spectrum from the inflationary axion-$U(1)$ spectator model with the parameter δ, the fine structure constant α of the $U(1)$ sector and the Hubble rate H satisfying $\delta = 0.5$, $24.0 < \alpha < 24.8$ and $H = 2.44 \cdot 10^{13}$GeV is plotted on top of the PTA data collected by the NANOGrav collaboration without performing a data analysis. This result is presented in Fig.1 given in the Introduction. From Fig.1, [17] claims that the GW spectrum produced by the inflationary

axion-$U(1)$ spectator model can explain PTA data. It also claims that the GW spectrum produced by the inflationary axion-$U(1)$ spectator model gives a better fit to PTA data than the SMBHB power-law model and gives even a better fit to PTA data if added to the SMBHB power-law model. Therefore, this work motivates to perform a proper data analysis of PTA data for the inflationary axion-$U(1)$ spectator model and to compare it to the SMBHB power-law model.
The code used to perform a Bayesian statistical analysis is PTArcade. The 68% credible regions of the Bayesian statistical analysis of the inflationary axion-$U(1)$ spectator model and of the SMBHB power-law model with PTA data yield the following conclusions. In order for the GW spectrum produced by the inflationary axion-$U(1)$ spectator model to fit PTA data and improve the SMBHB power-law model, the parameter δ should be taken equal to 0.2. For this value of the parameter δ, $\Delta N = 17$ e-folds should separate the moment when the CMB scale leaves the horizon and the moment when the axion velocity is maximal. The fine structure constant α of the $U(1)$ sector should satisfy $46 < \alpha < 66$. In addition, the Hubble rate H should verify $7.73 \cdot 10^{11}\text{GeV} < H < 4.23 \cdot 10^{13}\text{GeV}$ but this constraint depends only on the choice of the prior distributions of the free parameters. On top, the fine structure constant α of the $U(1)$ sector should be related to the Hubble rate H via $\alpha = -4\log_{10}(1.68 \cdot 10^{-29}H^2) + 46$ and the height of the axion potential Λ^4 should verify $9.20 \cdot 10^{14}\text{GeV} < \Lambda < 1.16 \cdot 10^{16}\text{GeV}$. In other words, the Bayesian statistical analysis allows to conclude that for $\delta = 0.5$, the inflationary axion-$U(1)$ spectator model does not give a better fit to PTA data than the SMBHB power-law model, which goes against the claim from [17]. The Bayesian statistical analysis shows that for $\delta = 0.5$, the inflationary axion-$U(1)$ spectator model can explain PTA data if $\Delta N = 15$, $19.6 < \alpha < 28.4$, $7.73 \cdot 10^{11}\text{GeV} < H < 4.23 \cdot 10^{13}\text{GeV}$, $\alpha = -1.76\log_{10}(1.68 \cdot 10^{-29}H^2) + 19.6$ and $1.16 \cdot 10^{15}\text{GeV} < \Lambda < 2.06 \cdot 10^{16}\text{GeV}$. The bounds on the parameters α and H overlap the values chosen in [17]. Therefore the results of this work agree with [17] in the sense that for $\delta = 0.5$ the GW spectrum produced by the inflationary axion-$U(1)$ spectator model could explain PTA data. However, as already pointed out, this choice of parameters does not improve the SMBHB power-law model, going against the claim of [17].
The Bayesian statistical analysis also yields the conclusion that if the parameter δ is set to 0.2, in order for the inflationary axion-$U(1)$ spectator model together with the SMBHB power-law model to fit PTA data, the parameters ΔN, α, H and Λ^4 must be subjects to the same constraints as in the case of the inflationary axion-$U(1)$ spectator model alone. The parameters A and γ of the SMBHB power-law contribution are not constrained. If the parameter δ is set to 0.5, in order for the inflationary axion-$U(1)$ model together with the SMBHB power-law model to fit PTA data, the parameters ΔN, α, H and Λ^4 are not constrained but the region $\gamma > 5, \log_{10}(A) < -15$ should be excluded. In addition, the Bayesian statistical analysis allows to conclude that for both value of the parameter δ, the inflationary axion-$U(1)$ spectator model together with the SMBHB power-law model gives a better fit to PTA data than the SMBHB power-law model alone. This conclusion is consistent with the claim of [17]. Finally, the Bayesian statistical analysis indicates that amongst all the models tested, the inflationary axion-$U(1)$ spectator model together with the SMBHB power-law model with $\delta = 0.2$ is the one that improves the most the SMBHB power-law model.
As a conclusion, this work suggests some clear next steps for the future. In order for the inflationary axion-$U(1)$ spectator model to fit PTA data and improve the SMBHB power-law model, a preferred value of the parameter δ clearly appears. This result suggests to perform the analysis presented in this work for a wider range of values for the parameter δ, in order to quantify for which range of values of the parameter δ the inflationary axion-$U(1)$ spectator model can fit PTA data and improve the SMBHB power-law model. Then, as for $\delta = 0.5$ the run of the inflationary axion-$U(1)$ spectator model together with the SMBHB power-law model allows values of the free parameter f_* at high frequencies for which no PTA data exist, it would be interesting to re-launch the run with a more restrictive prior distribution of the parameter f_*. Moreover, in a recent work from Ogan Ozsoy, Alexandros Papageorgiou and Matteo Fasiello [35] the validity of using a log-normal form for the normalization factor that enters in the gauge field solution has been studied. It is shown that using such a log-normal form leads to underestimate the amplitude of the GWs produced. This consideration together with the fact that the solution of the gauge field is obtained via an approximation yield a clear next step for this project: solve the equation of motion of the gauge field numerically. However, the statement from [35] as well as the calculation of the solution for the gauge field strongly depend on the integration domain over the comoving wavenumber k. Particularly, one has to introduce a cutoff in order for the integral not to diverge so that the statement from [35] and the calculation of the solution for the gauge field strongly depend on this cutoff. Physically, this cutoff represents the transition from vacuum to sourced perturbations, which is not clearly defined. So solving the equation of motion of the gauge field numerically and derive a proper cutoff from quantum field theory simultaneously would be a next step. Finally, all the results from the Bayesian statistical analysis lie close to the low-backreaction regime bound. Therefore, it would be interesting in future to re-do the analysis presented in this work in the strong backreaction regime. This would require to solve non-linear coupled differential equations and a possible way to perform such an analysis could be to use the "Gradient expansion formalism" developed by the Münster group that aims to solve numerically such sets of differential equations [36–38].

Appendices

A Derivation of the sourced contribution of the tensor power spectrum

This appendix presents the derivation of the sourced contribution of the tensor power spectrum given in Eq. (3.16).
From the definition of the tensor power spectrum given in Eq. (3.14), the sourced contribution of the tensor power spectrum is given by:

$$\mathcal{P}_\lambda(k)\delta_{\lambda\lambda'}\delta^{(3)}(\vec{k}+\vec{k'}) \equiv \frac{k^3}{2\pi^2}\langle 0|\hat{h}^{(1)}_\lambda(\tau,\vec{k})\hat{h}^{(1)}_{\lambda'}(\tau,\vec{k'})|0\rangle, \tag{A.1}$$

with

$$\begin{aligned}\langle 0|\hat{h}^{(1)}_\lambda(\tau,\vec{k})\hat{h}^{(1)}_{\lambda'}(\tau,\vec{k'})|0\rangle =& \frac{2H^4}{M_P^4}\frac{\Pi_{ij,\lambda}(\hat{k})\Pi_{ij,\lambda'}(\hat{k'})}{k^{7/2}k'^{7/2}}\int\frac{d^3p_1}{(2\pi)^{3/2}}p_1^{1/4}|\vec{k}-\vec{p_1}|^{1/4}N\left[\frac{p_1}{k_*},\xi_*,\delta\right]N\left[\frac{|\vec{k}-\vec{p_1}|}{k_*},\xi_*,\delta\right]T\left[x_*,\xi_*,\delta,\frac{p_1}{k},\frac{|\vec{k}-\vec{p_1}|}{k}\right]\\
&\cdot\left[\epsilon_i^+(\hat{p_1})\hat{a}_+(\vec{p_1})+\epsilon_i^{+*}(-\hat{p_1})\hat{a}_+^\dagger(-\vec{p_1})\right]\left[\epsilon_j^+(\hat{k}-\hat{p_1})\hat{a}_+(\vec{k}-\vec{p_1})+\epsilon_j^{+*}(-\hat{k}+\hat{p_1})\hat{a}_+^\dagger(-\vec{k}+\vec{p_1})\right]\\
&\cdot\int\frac{d^3p_2}{(2\pi)^{3/2}}K_\lambda[\hat{k'},\hat{p_2},\hat{k'}-\hat{p_2}]p_2^{1/4}|\vec{k'}-\vec{p_2}|^{1/4}N\left[\frac{p_2}{k'_*},\xi_*,\delta\right]N\left[\frac{|\vec{k'}-\vec{p_2}|}{k'_*},\xi_*,\delta\right]T\left[x'_*,\xi_*,\delta,\frac{p_2}{k'},\frac{|\vec{k'}-\vec{p_1}|}{k'}\right]\\
&\cdot\left[\epsilon_i^+(\hat{p_2})\hat{a}_+(\vec{p_2})+\epsilon_i^{+*}(-\hat{p_2})\hat{a}_+^\dagger(-\vec{p_2})\right]\left[\epsilon_j^+(\hat{k'}-\hat{p_2})\hat{a}_+(\vec{k'}-\vec{p_2})+\epsilon_j^{+*}(-\hat{k'}+\hat{p_2})\hat{a}_+^\dagger(-\vec{k'}+\vec{p_2})\right],\end{aligned} \tag{A.2}$$

where the function T is defined in Eq. (3.13). Using the commutation relation of the gauge field creation and annihilation operators, the non-vanishing contributions in terms of creation and annihilation operators are:

$$\langle 0|a_\lambda(\vec{p_1})a_\lambda(\vec{k}-\vec{p_1})a^\dagger_{\lambda'}(-\vec{p_2})a^\dagger_{\lambda'}(-\vec{k'}+\vec{p_2})|0\rangle \quad \langle 0|a_\lambda(\vec{p_1})a^\dagger_\lambda(-\vec{k}+\vec{p_1})a_{\lambda'}(\vec{p_2})a^\dagger_{\lambda'}(-\vec{k'}+\vec{p_2})|0\rangle, \tag{A.3}$$

that lead to three contributions given by:

$$\delta_{\lambda\lambda'}\delta^{(3)}(\vec{p_1}+\vec{p_2})\delta^{(3)}(\vec{k}+\vec{k'}) \quad \delta_{\lambda\lambda'}\delta^{(3)}(\vec{k}-\vec{p_1}+\vec{p_2})\delta^{(3)}(\vec{p_1}+\vec{k'}-\vec{p_2}) \quad \delta_{\lambda\lambda'}\delta^{(3)}(\vec{k})\delta^{(3)}(\vec{k'}). \tag{A.4}$$

The second contribution reads $\delta_{\lambda\lambda'}\delta^{(3)}(\vec{k}+\vec{k'})\delta^{(3)}(\vec{p_1}-\vec{k}-\vec{p_2})$. From the dependencies of the four normalization factors in Eq. (A.2) it is possible to show that taking $\vec{k}=\vec{k'}$ and $\vec{p_2}=\vec{p_1}-\vec{k}$ or $\vec{k}=\vec{k'}$ and $\vec{p_2}=-\vec{p_1}$ gives the same four resulting normalization factors. In addition, from the definition of the function T given in Eq. (3.13), exchanging the order of the two last arguments does not change the result. This means that in Eq. (A.2), taking $\vec{k}=\vec{k'}$ and $\vec{p_2}=\vec{p_1}-\vec{k}$ or $\vec{k}=\vec{k'}$ and $\vec{p_2}=-\vec{p_1}$ gives the same two resulting functions T. Finally, the contribution $\delta_{\lambda\lambda'}\delta^{(3)}(\vec{k})\delta^{(3)}(\vec{k'})$ is non-zero only when $\vec{k}=\vec{k'}=\vec{0}$ that correspond to infinite wavelengths that are unobservable and therefore disregarded. To sum up, the three contributions given in Eq. (A.4) give two times the same contribution.
The resulting correlator of the sourced contribution of the tensor perturbations then reads:

$$\begin{aligned}\langle 0|\hat{h}^{(1)}_\lambda(\tau,\vec{k})\hat{h}^{(1)}_{\lambda'}(\tau,\vec{k'})|0\rangle =& \delta_{\lambda\lambda'}\delta^{(3)}(\vec{k}+\vec{k'})\frac{4H^4}{M_P^4k^7}\Pi_{ij,\lambda}(\hat{k})\Pi_{ij,\lambda'}(\hat{k})\int\frac{d^3p}{(2\pi)^3}\epsilon_i^+(\hat{p_1})\epsilon_j^+(\hat{k}-\hat{p_1})\epsilon_i^{+*}(\hat{p_1})\epsilon_j^{+*}(\hat{k}-\hat{p_1})\sqrt{p|\vec{k}-\vec{p}|}\\
&\cdot N^2\left[\frac{p}{k_*},\xi_*,\delta\right]N^2\left[\frac{|\vec{k}-\vec{p}|}{k_*},\xi_*,\delta\right]T^2\left[x_*,\xi_*,\delta,\frac{p}{k},\frac{|\vec{k}-\vec{p}|}{k}\right],\end{aligned} \tag{A.5}$$

with

$$\Pi_{ij,\lambda}(\hat{k})\Pi_{ij,\lambda'}\epsilon_i^+(\hat{p_1})\epsilon_j^+(\hat{k}-\hat{p_1})\epsilon_i^{+*}(\hat{p_1})\epsilon_j^{+*}(\hat{k}-\hat{p_1}) = \epsilon_i^\lambda(\hat{k})\epsilon_i^{+*}(\hat{p_1})\epsilon_i^+(\hat{p_1})\epsilon_i^{\lambda'*}(\hat{k})\epsilon_j^\lambda(\hat{k})\epsilon_j^{+*}(\hat{k}-\hat{p_1})\epsilon_j^+(\hat{k}-\hat{p_1})\epsilon_j^{\lambda'*}(\hat{k}). \tag{A.6}$$

In order to compute the scalar product of the circular polarization vectors, one has to go back to the definition of circular polarization vectors. For a mode of momentum p, a choice for the linear polarization vectors can be:

$$\vec{\epsilon}^{(2)}(\vec{p}) = \frac{\vec{l}\times\vec{p}}{|\vec{l}\times\vec{p}|} \quad \vec{\epsilon}^{(1)}(\vec{p}) = \frac{\vec{\epsilon}^{(2)}(\vec{p})\times\vec{p}}{p}, \tag{A.7}$$

where $\vec{l}$ is a vector not colinear to $\vec{p}$. The circular polarization vectors are then defined as:

$$\vec{\epsilon}^\lambda \equiv \frac{1}{\sqrt{2}}\left[\vec{\epsilon}^{(1)}(\vec{p})+i\lambda\vec{\epsilon}^{(2)}(\vec{p})\right]. \tag{A.8}$$

For a pair of momenta p and p', choosing the same $\vec{l}$ to construct the circular polarization vectors as $\vec{l}=\vec{p}\times\vec{p'}$ it can be shown that (see [39] Appendix D):

$$\vec{\epsilon}^{\lambda*}(\vec{p})\cdot\vec{\epsilon}^{\lambda'}(\vec{p'}) = \frac{1}{2}(1+\lambda\lambda'\hat{p}\cdot\hat{p'}). \tag{A.9}$$

Using this trick in Eq. (A.8), putting everything together and introducing $\vec{q}\equiv\vec{p}/k$ the sourced contribution of the tensor power spectrum can be written as in Eq. (3.16).

B Prior distribution of the free parameters from the gravitational wave spectrum of supermassive black hole binaries

The prior distribution of the free parameters A and γ of the SMBHB power-law model used in PTArcade are the black dashed lines presented in Fig.6.

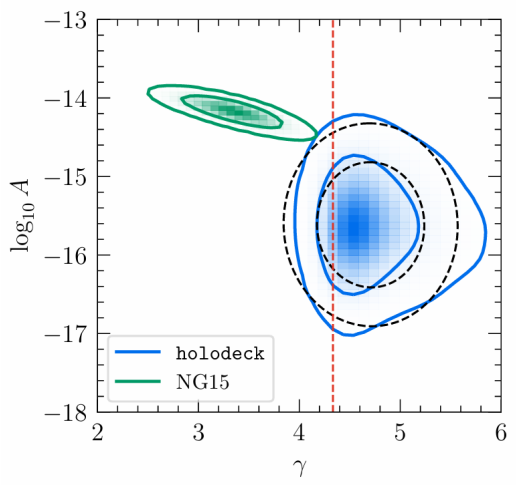

Figure 6: The contours of interest for this work are the blue contours. They are the comparison of the 68% and 95% probability regions for the amplitude A and slope γ of a power-law fit predicted for purely GW-driven SMBHB populations by the NANOGrav collaboration. The black dashed lines represent a 2D Gaussian fit of the blue contours. The vertical red line indicates $\gamma = 13/3$, the naive expectation for a GWB produced by a GW-driven SMBHB population [29]

References

[1] G. Agazie and al. (NANOGrav) "The NANOGrav 15-year Data Set: Evidence for a Gravitational-Wave Background", *Astrophys. J. Lett.*, **951** (2023)

[2] Nihan S. Pol and al. "Astrophysics Milestones For Pulsar Timing Array Gravitational Wave Detection", *The Astrophys. J. Lett.*, **911** (2021)

[3] Adeela Afzal et al. "The NANOGrav 15 yr Data Set: Search for Signals from New Physics" *Astrophys.J.Lett.* **951** (2023)

[4] A. Riotto "Inflation and the Theory of Cosmological Perturbations" arXiv:1010.2642v3

[5] A. A. Starobinsky "Spectrum of relict gravitational radiation and the early state of the universe" *JETP Lett.* **30** (1979)

[6] A. H. Guth "The Inflationary Universe: A Possible Solution to the Horizon and Flatness Problems" *Phys. Rev.* **D 23** (1981)

[7] A. D. Linde "A New Inflationary Universe Scenario: A Possible Solution of the Horizon, Flatness, Homogeneity, Isotropy and Primordial Monopole Problems" *Phys. Lett.* **B 108** (1982)

[8] R. D. Peccei, H. R. Quinn "CP Conservation in the Presence of Instantons" *Phys. Rev. Lett.* **38** (1977)

[9] R. D. Peccei, H. R. Quinn "Constraints Imposed by CP Conservation in the Presence of Instantons" *Phys. Rev.* **D 16** (1977)

[10] S. Weinberg "A New Light Boson?" *Phys. Rev. Lett.* **40** (1978)

[11] F. Wilczek "Problem of Strong P and T Invariance in the Presence of Instantons" *Phys. Rev. Lett.* **40** (1978)

[12] L. Sorbo "Parity violation in the Cosmic Microwave Background from a pseudoscalar inflaton" *JCAP* **06** (2011)

[13] N. Barnaby, R. Namba, M. Peloso "Phenomenology of a Pseudo-Scalar Inflaton: Naturally Large Nongaussianity" *JCAP* **009** (2011)

[14] R. Z. Ferreira, M. S. Sloth "Universal Constraints on Axions from Inflation" *JHEP* **12** (2014),

[15] V. Domcke, M. Pieroni, and P. Binétruy, "Primordial gravitational waves for universality classes of pseudoscalar inflation" *JCAP* **031** (2016)

[16] O. Ozsoy "Synthetic Gravitational Waves from a Rolling Axion Monodromy" *JCAP* **040** (2021)

[17] Caner Unal, Alexandros Papageorgiou, Ippei Obata, "Axion-Gauge Dynamics During Inflation as the Origin of Pulsar Timing Array Signals and Primordial Black Holes", arXiv:2307.02322 (2023)

[18] R. Namba, M. Peloso, M. Shiraishi, L. Sorbo and C. Unal "Scale-dependent gravitational waves from a rolling axion", *JCAP* **01** (2016)

[19] Michael S. Turner, Lawrence M. Widrow "Inflation Produced, Large Scale Magnetic Fields", *Phys.Rev.* **D37** (1988)

[20] W.Daniel Garretson, George B. Field, Sean M. Carroll "Primordial magnetic fields from pseudoGoldstone bosons", *Phys.Rev.* **D46** (1992)

[21] E. Merzbacher "Quantum mechanics" *Wiley* (1997)

[22] M. Sasaki "Large Scale Quantum Fluctuations in the Inflationary Universe" *Progress of Theoretical Physics* **76** (1986)

[23] V.F. Mukhanov, H.A. Feldman, and R.H. Brandenberger "Quantum Theory of Gauge Invariant Cosmological Perturbations" *Physics Reports* **215** (1992)

[24] P. Campeti, O. Özsoy, I. Obata, M. Shiraishi "New constraints on axion-gauge field dynamics during inflation from Planck and BICEP/Keck data sets" *JCAP* **07** (2022)

[25] M. Peloso, L. Sorbo, C. Unal "Rolling axions during inflation: perturbativity and signatures" *JCAP* **09** (2016)

[26] Planck Collaboration "Planck 2018 results. X. Constraints on inflation" *Astron.Astrophys.* **641** (2020)

[27] D. Baumann "Cosmology" *Cambridge University Press* (2022)

[28] S. R. Taylor "The Nanohertz Gravitational Wave Astronomer" arXiv:2105.13270

[29] NANOGrav collaboration "The NANOGrav 15-year Data Set: Search for Signals from New Physics" arXiv:2306.16219v1

[30] BICEP/Keck Collaboration "BICEP / Keck XIII: Improved Constraints on Primordial Gravitational Waves using Planck, WMAP, and BICEP/Keck Observations through the 2018 Observing Season" *Phys. Rev. Lett.* **127** (2021)

[31] A. Mitridate, D. Wright, R. v. Eckardstein, T. Schröder, J. Nay, K. Olum, K. Schmitz, T. Trickle "PTArcade" arXiv:2306.16377

[32] A. Mitridate PTArcade website https://andrea-mitridate.github.io/PTArcade/

[33] B. Efron, R. Tibshirani "Bootstrap Methods for Standard Errors, Confidence Intervals, and Other Measures of Statistical Accuracy" *Statist. Sci.* **57** (1986)

[34] M. Peloso, L. Sorbo, C. Unal "Rolling axions during inflation: perturbativity and signatures" *JCAP* **09** (2016)

[35] O. Özsoy, A. Papageorgiou, M. Fasiello "Scale-dependent chirality as a smoking gun for Abelian gauge fields during inflation" arXiv:2405.14963

[36] E. V. Gorbar, K. Schmitz, O. O. Sobol, S. I. Vilchinskii, "Gauge-field production during axion inflation in the gradient expansion formalism" *Phys. Rev.* **D 104** (2021)

[37] O. O. Sobol, E. V. Gorbar S. I. Vilchinskii "Backreaction of electromagnetic fields and the Schwinger effect in pseudoscalar inflation magnetogenesis" *Phys. Rev.* **D 100** (2019)

[38] O. O. Sobol, A. V. Lysenko, E. V. Gorbar S. I. Vilchinskii "Gradient expansion formalism for magnetogenesis in the kinetic coupling model" *Phys. Rev.* **D 102** (2020)

[39] R. Durrer, R. von Eckardstein, Deepen Garg, K. Schmitz, O. Sobol, S. Vilchinskii "Scalar perturbations from inflation in the presence of gauge fields" arXiv:2404.19694 (2024)